HEDL-TME 72-42
APRIL 1972

Three Dimensional Neutronics Calculations For The Fast Test Reactor (FTR) and The FTR Engineering Mock Up Critical Assembly (EMC)

Hanford Engineering Development Laboratory

Contract:
AT(45-1)-2170

NOTICE

Hanford Engineering Development Laboratory

Operated by the
Westinghouse
Hanford Company

A Subsidiary of
Westinghouse Electric
Corporation

for the United States
Atomic Energy Commission
Contract No. AT(45-1)-2170

P.O. Box 1970 Richland, Wa. 99352

AEC-RL RICHLAND, WASH

HEDL-TME 72-42
APRIL 1972

THREE DIMENSIONAL NEUTRONICS CALCULATIONS FOR THE FAST TEST REACTOR (FTR) AND THE FTR ENGINEERING MOCK UP CRITICAL ASSEMBLY (EMC)

R.M. Fleischman
J.V. Nelson

HANFORD ENGINEERING DEVELOPMENT LABORATORY

UNITED STATES ATOMIC ENERGY COMMISSION

CONTRACT AT(45-1)-2170

Blank Page

ABSTRACT

The three-dimensional diffusion theory code, 3DB, was used to make full-core, detailed, thirty energy group, neutronics calculations of the FTR and EMC. Eigenvalue and reaction rate distribution calculations for the EMC are presented and the latter are compared with experiment. The FTR criticality search using target eigenvalues derived from EMC calculations and calculation of the FTR Doppler coefficient in the established critical configuration are discussed. Finally, reaction rate and power distributions and neutron energy spectra from FTR calculations are presented. Appended to the report are complete cross section and three-dimensional modeling details, and a discussion of 3DB convergence behavior.

Blank Page

ACKNOWLEDGEMENTS

The authors wish to acknowledge R. W. Hardie for his assistance in the initial phases of performing these calculations and the efforts of W. W. Little, Jr. and Mr. Hardie in modifying the 3DB code for operation on the CDC 7600 computer. The assistance of the computer operations organization at Lawrence Berkeley Laboratory and in particular the attention and patience of M. Atchley and E. Beals are gratefully acknowledged.

Blank Page

TABLE OF CONTENTS

Blank Page

LIST OF FIGURES

Blank Page

LIST OF FIGURES (Cont'd)

Blank Page

LIST OF TABLES

1.0 INTRODUCTION

Nuclear design calcuations for the Fast Test Reactor (FTR) currently utilize two-dimensional diffusion methods. The reactor models employed in these calculations are either (R,Z) with annularized control rods, safety rods and test loops, or hexagonal or (X,Y) geometries utilizing an axial buckling inferred from a previous (R,Z) calculation. Because of the pronounced heterogeneous nature of the FTR core, defining a satisfactory two-dimensional model is somewhat arbitrary and often involves a considerable number of sensitivity studies to evaluate the effect of various assumptions and approximations on the parameter(s) of interest. The obvious alternative to two-dimensional design calculations is a straight forward use of three-dimensional analysis for all reactor design computations, or at least the use of selected three-dimensional benchmark calculations for the development of more reliable and less expensive two-dimensional techniques. This approach was not adopted in the past because of anticipated difficulties with convergence of large, many-group three-dimensional calculations coupled with long running times and limited computer capabilities. These difficulties have now been overcome at least in part and bona fide 3D analyses are now feasible.

This report summarizes detailed three-dimensional neutronic calculations of the FTR and the FTR Engineering Mockup Critical performed with the diffusion theory burnup program 3DB[1]. These calculations demonstrate the feasibility and value of three-dimensional analysis for fast reactor core design.

2.0 SUMMARY AND CONCLUSIONS

3DB[1] was used to make detailed full core neutronics calculations of the FTR as well as the FTR Engineering Mockup Critical (EMC). For all calculations, the FTR Design Set 300 cross sections[2] were resonance self shielded and collapsed in the one-dimensional diffusion theory cross section preparation program IDX[3]. The calculations were performed at the Lawrence Berkeley Laboratory on the CDC 7600 computer.

The EMC three-dimensional model contained 33 (X) x 33(Y) x 38(Z) dimensional mesh, 88 material zones, and cross sections for 34 input materials. The calculated eigenvalues for the EMC were respectively 0.97838 and 0.97868 for four and thirty energy group homogeneously resonance self shielded cross sections. Starting from flux shapes which were peaked in the core center and decreased linearly to near zero at the model edge, the four and thirty group problems converged to 4.4×10^{-5} and 7×10^{-5} in 36 and 206 minutes respectively. These running times are considered to be quite practical for design calculations.

Critical FTR target eigenvalues of .98898 and .98928 for four and thirty groups, respectively, were inferred from EMC calculations, a calculated heterogeneity correction (.0116 Δk) [4] and the experimental k_{eff} of 1.001. Target eigenvalues were sought by manually adjusting the FTR control rod settings in four group calculations. The best critical rod position was established with a thirty energy group calculation having all control rods inserted 16 inches (k=.9889). This FTR calculation provided heretofore unavailable axial definition of off-axis reaction rates, power districutions, axial power peaking factors and neutron spectral effects which are presented in the main body of this report.

The three-dimensional model employed in FTR calculations contained 51 x 30 (hexagonal) x 27 (Z) dimensional mesh, 79 material zones, and cross sections for 34 input materials. Starting from flux shapes similar to those used in EMC calculations, the four group cases converged to 1×10^{-5} in 27 minutes. The thirty group calculation converged to 4.7×10^{-5} in 80 minutes when started with a four group flux expanded to 30 groups in the reverse order of cross section collapsing. Again, these running times are quite practical for design calculations.

The 3D analysis was also used to determine the Doppler constant for the FTR. A Doppler constant of T dk/dT= -.00525 was calculated for the fuel enrichment and reactor configuration studied. This Doppler coefficient calculation was repeated using two-dimensional techniques and excellent agreement with three-dimensional results was achieved.

In general, it was concluded that three-dimensional multigroup analyses are a practical design tool for fast reactor analysis. Judicious choice of both 3D and 2D calculations can be used to advantage in obtaining accurate nuclear design data at reasonable computing costs.

3.0 CALCULATIONS FOR THE ENGINEERING MOCKUP CRITICAL (EMC)

3.1 Eigenvalue Calculations - The FTR Engineering Mockup Critical (EMC) Beginning of Life (BOL) configuration as constructed in ZPR-9, was analyzed in three dimensional x, y and z geometry. Calculations were performed using both 30 and 4 energy group homogeneously resonance self shielded cross sections. The details of the cross section preparation scheme are discussed in Appendix A.

The EMC core map is shown in Figure 3.1.1. The configuration considered contained three peripheral shim rods (702, 714, 726), three inserted control rods (508, 516, 524), three withdrawn control rods (506, 514, 522), three material test shims (401, 407, 413), three withdrawn safety rods (304, 308, 312), four closed loops (201, 403, 415, 625) and one withdrawn oscillator (203). The axial definition achieved in the EMC 3DB model is briefly described in Figure 3.1.2. A more complete description of the EMC 3DB model is given in Appendix B.

The calculated eigenvalues for the EMC-BOL were .97838 and .97868 for four and thirty energy groups respectively. The convergence behavior of these calculations and the method of arriving at these eigenvalues are discussed in Appendix D.

The experimental eigenvalue for the EMC-BOL configuration is 1.001 [5] and the platelet heterogeneity correction is 0.0116 Δk. [4] These values were used to establish the FTR design bias factors as follows:

$$B_4 = 1.001 - (.97838 + .0116) = .01102$$
$$k_4^T = 1 - B_4 = .98898$$
$$B_{30} = 1.001 - (.97868 + .0116) = .01072$$
$$k_{30}^T = 1 - B_{30} = .98928$$

where B_n is the bias factor for n energy groups and k_n^T is the eigenvalue to be calculated in the FTR for a critical configuration using n energy group, heterogeneously resonance self shielded, cross sections. These "target eigenvalues" were used for the FTR criticality search discussed in Section 4.1.

3.2 Reaction Rate Distributions - As part of the EMC experiments, radial distributions of ^{239}Pu (n,f), ^{238}U (n,f), and ^{10}B (n,α) reaction rates[5], and the axial distribution of ^{239}Pu (n,f) reaction rate were measured with detectors. In addition, an axial center line distribution and a 1/3 core midplane map of the ^{239}Pu fission rate were measured using fission foils[6].

Comparisons of normalized axial and radial reaction rate data with results from three-dimensional calculations are given in Figures 3.2.1 through 3.2.4. Where both foil and detector data are available, both are plotted and noted on the figure.

The calculated ^{238}U (n,f) and ^{10}B (n,α) reaction rate distributions were significantly perturbed in the safety rod channel whereas measured reaction rates were not affected by this sodium-stainless steel region.

Calculations of the ^{239}Pu fission rate display much closer agreement with foil data near the core reflector boundaries. One possible explanation of this is that the current data are subject to neutron streaming in the traverse tube, whereas foils are introduced into the reactor without this perturbation. Even so, the plutonium fission rate, when compared to foil data, is still undercalculated indicating an on-going difficulty with calculating the rapidly softening energy spectrum at the reflector boundary. This effect is most pronounced at the radial reflector boundary where the spectral shift is the greatest.

Figure 3.2.5 shows the XY map (see Figure 3.1.1) of foil locations used to make an approximate 1/3 core map the the core axial midplane. The ratio of calculated to experimental reaction rates normalized to unity at the core center are given for each foil location. These comparisons have the shortcoming that reaction rates calculated from a homogeneous core representation using homogeneous cross sections are being compared to experimental reaction rates which are sensitive to neutron flux fine structure in the two-drawer EMC core cells. Shielding effects in the plutonium foils have also been ignored. These effects are the suspected origin of the left-to-right oscillatory nature of the C/E values in the core regions. Despite these shortcomings, the systematic undercalculation of the fission rate near the reflector and over-calculation near inserted control and peripheral shim rods is apparent from the figure.

If the measured foil data are treated as indicative of the average ^{239}Pu fission rate in a homogeneous system, then by adjusting for inner core-outer core plutonium density differences, an experimental average power density and thus power peaking factor can be easily inferred. Following the same prescription with the calculated reaction rates, the experimental and calculated peaking factors can be compared as a test of the calculational model.

Experimental and calculated power peaking factors inferred from these data are 1.3898 and 1.3843 respectively, and the C/E value is 0.996. This agreement is quite good; however, a more sophisticated analytical treatment of this experiment is appropriate before final conclusions can be drawn.

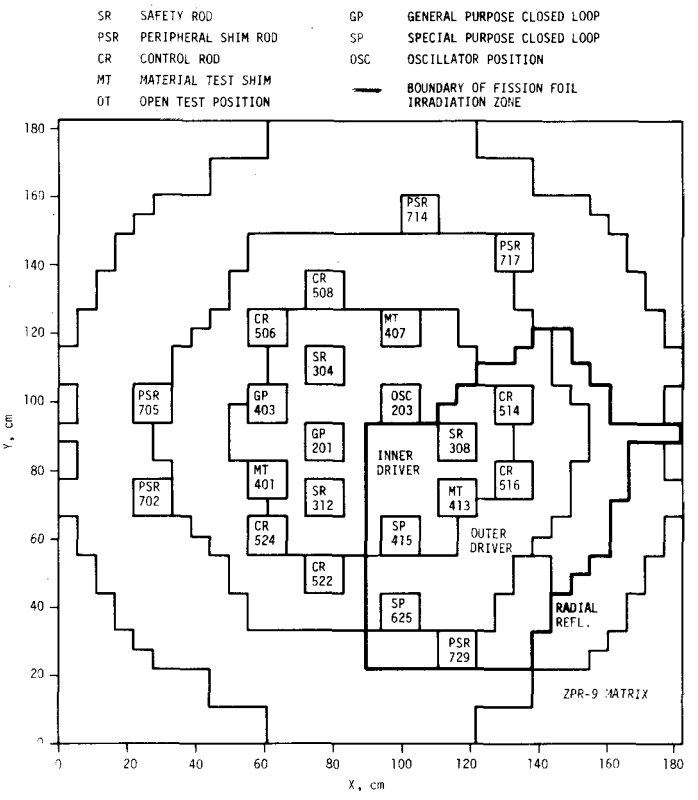

Figure 3.1.1 EMC XY Map

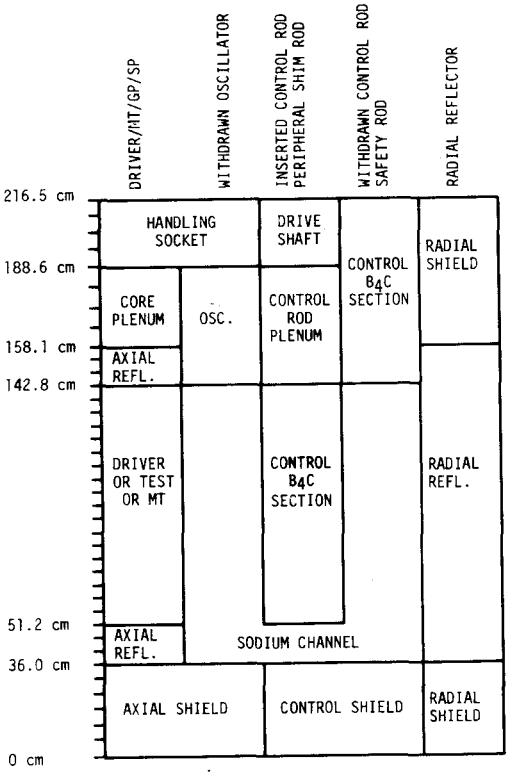

Figure 3.1.2 EMC 3DB Axial Model

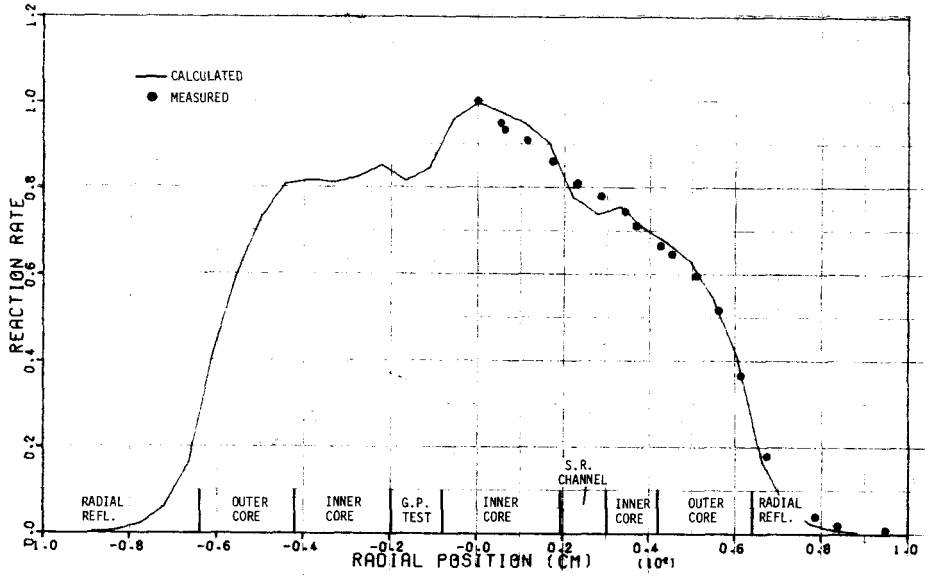

Figure 3.2.1 EMC-BOL, ^{238}U Radial Fission Rate Distribution

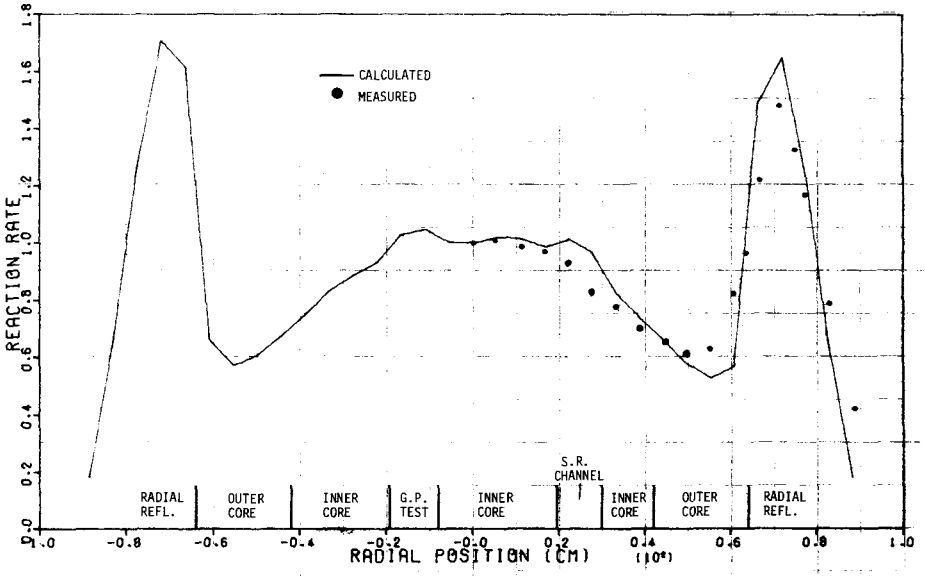

Figure 3.2.2 EMC-BOL, Radial ^{10}B (n, α) Reaction Rate Distribution

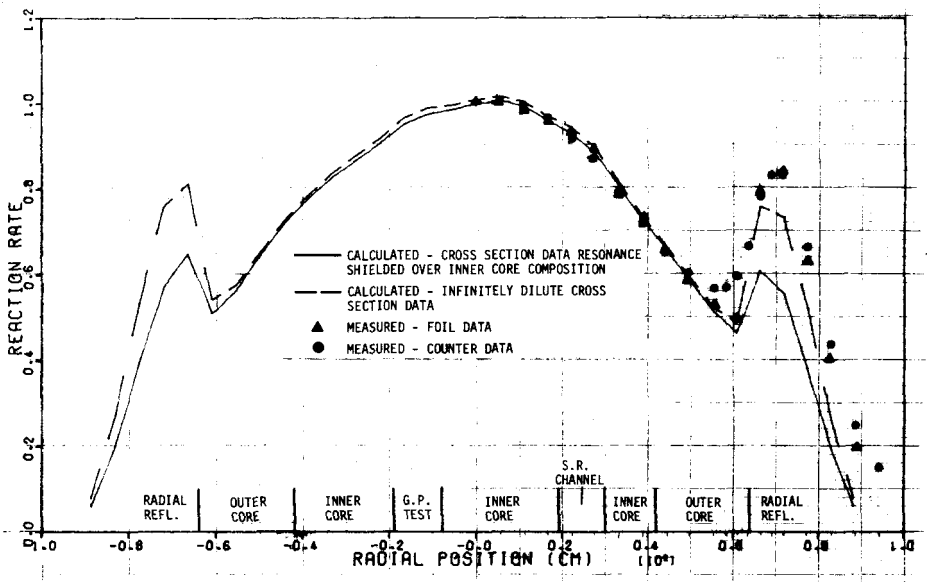

Figure 3.2.3 EMC-BOL, Radial ^{239}Pu Fission Rate Distribution

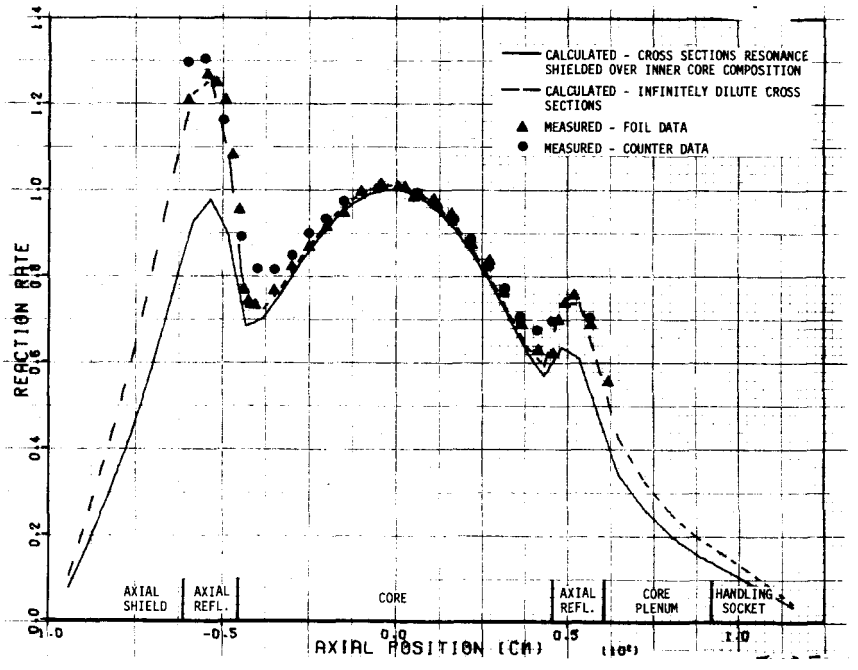

Figure 3.2.4 EMC-BOL, Axial ^{239}Pu Fission Rate Distribution

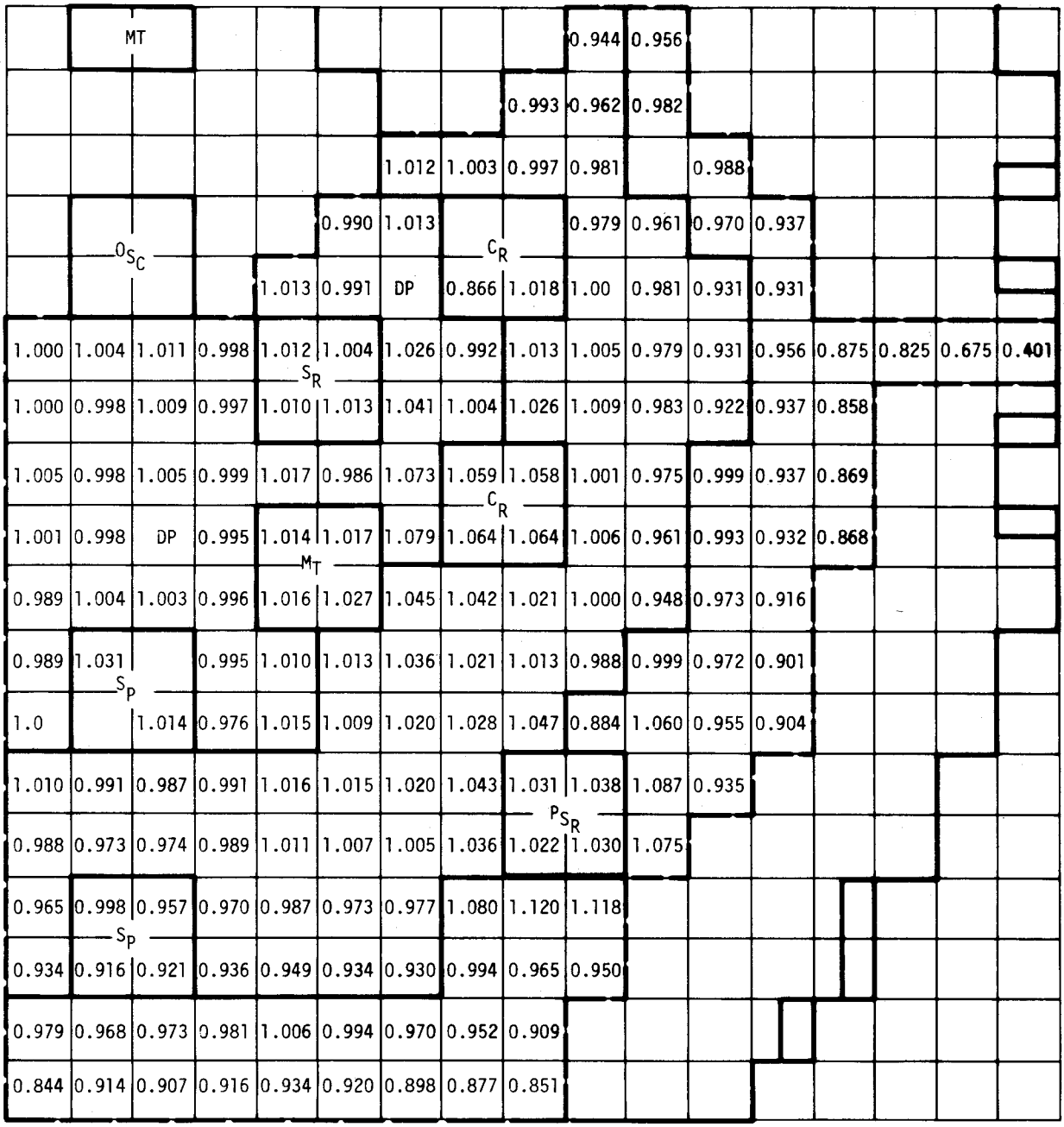

Figure 3.2.5 EMC 1/3 Core Fission Irradiations Map (c/e values)

4.0 CALCULATIONS FOR FTR

4.1 Criticality Search - The FTR Beginning of Life (BOL) configuration was analyzed in three dimensional Hex.-Z geometry. Calculations were performed using both 30 and 4 energy group, heterogenously resonance self shielded cross sections. The specific cross section preparation scheme is discussed in Appendix A. "Target eigenvalues" derived from three-dimensional EMC calculations were used to search for a "critical" control rod configuration in the FTR-BOL.

The FTR core map is shown in Figure 4.1.1. The BOL configuration calculated contained three peripheral shim rods (702, 714, 726), three material test shims (401, 407, 413), three withdrawn safety rods (304, 308, 312), four closed loops (201, 403, 414, 625), a material test in an open test position (203), driver assemblies in the remaining test positions, and a variable setting on the row five control rods. The axial definition achieved in the FTR-3DB model is briefly described in Figure 4.1.2. A more complete description of the FTR 3DB model and densitites is given in Appendix C.

The calculated eigenvalues for various control rod settings selected in the FTR criticality search are given in Table 4.1.1. The four group calculations defined a critical configuration with five control rods set at 16 inches and one at 18 inches. This configuration was then calculated in thirty groups. One slight control rod movement (all rods at 16 inches) was necessary in order to achieve criticality in 30 energy groups, indicating that the four group cross section set is quite good for eigenvalue calculations.

The criticality search calculations which extended over several weeks were complicated by changes in the FTR fuel enrichment which occurred during that time period. Calculations performed with "new" and "old" enrichments are identified in Table 4.1.1. Although the "new" enrichments most likely will not be those selected for the final FTR design (Appendix C), these calculations, nevertheless, do represent valuable models for testing calculational tools which are simpler and less expensive than three-dimensional analysis.

From the series of four group calculations, selected points of a control rod calibration curve may be inferred. Figure 4.1.3 represents an estimated control rod calibration curve with calculated points identified. In the maximum differential worth region the control rod worth is approximately 0.3% $\Delta k/k$/inch for all six rods banked, and the peak to average differential worth is nominally 1.5.

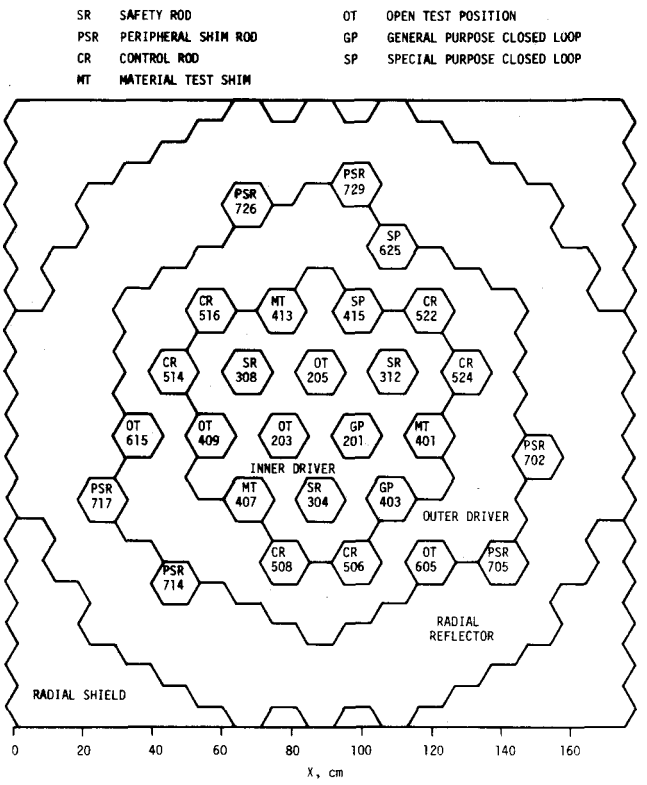

Figure 4.1.1 FTR Hex Map

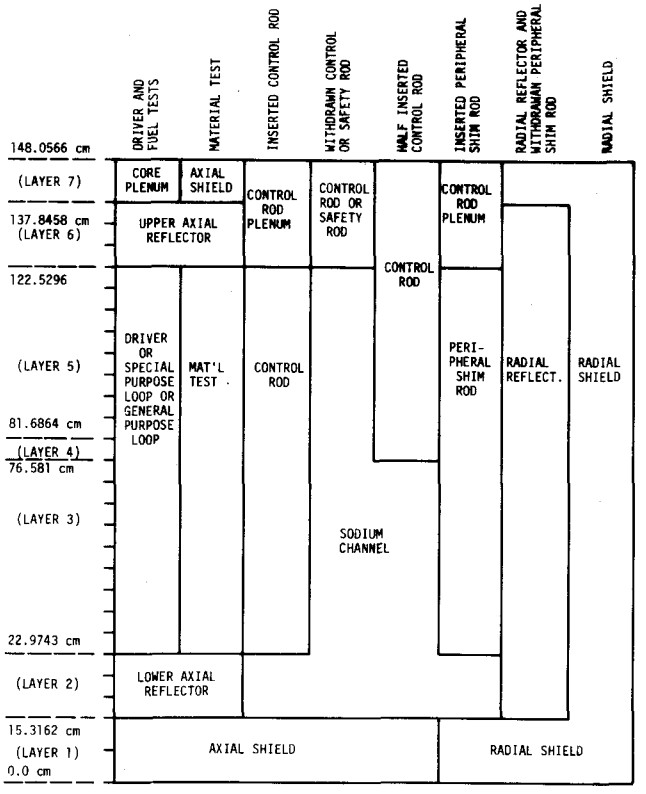

Figure 4.1.2 FTR 3DB Axial Model

TABLE 4.1.1

CALCULATIONS PERFORMED FOR FTR CRITICALITY SEARCH

Energy	CONTROL ROD INCHES INSERTED							
Group	506	508	514	516	522	524	Enrichment	Eigenvalue
4	0	0	0	0	0	0	OLD	1.01546
4	18	18	18	18	18	18	OLD	.98083
4	36	36	36	36	36	36	OLD	.94532
4	16	16	16	16	16	16	OLD	.98675
4	16	16	16	16	16	16	NEW	.98980
4	16	18	16	16	16	16	NEW	.98877
30	16	18	16	16	16	16	NEW	.9879
30	16	16	16	16	16	16	NEW	.9889

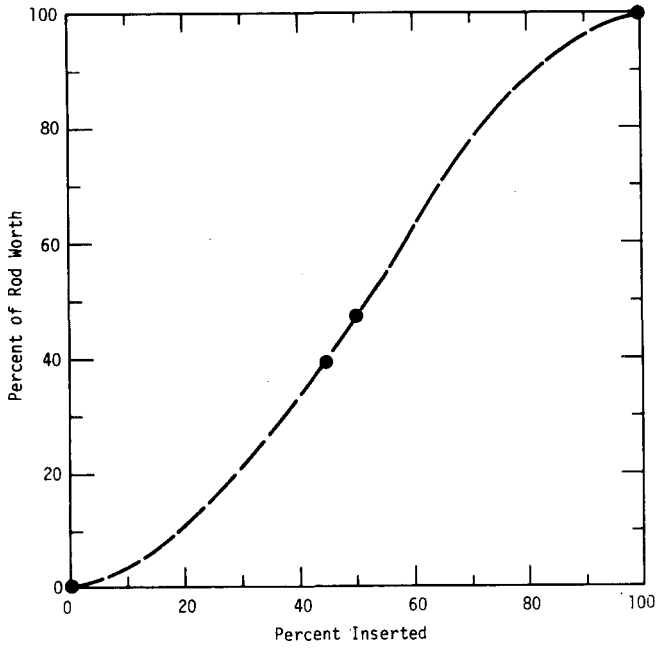

Figure 4.1.3 Estimated Row Five Control Rod Worth Profile

4.2 Doppler Coefficient Calculations - The Doppler coefficient of the critical FTR configuration was calculated for three different temperatures by changing the temperature of the ^{238}U isotope in the cross section set (Appendix A) and calculating the eigenvalue using these three different sets of cross sections. The temperature of the Pu cross sections was left unchanged since a positive plutonium Doppler effect is invariably calculated in contrast to experimental evidence which indicates that it is, in fact, small and negative[7,8].

Recent extensive sensitivity studies by the FTR core designer have led to the recommendation of a specific, relatively simple, and inexpensive two-dimensional (R,Z) representation of the FTR for Doppler calculations[9]. The basic features of the (R,Z) method are:

- rings of hexagonal drivers (and loops, etc.) are represented as cylindrical annuli of equal volume, with the exception of row 5 control rods.
- row 5 control rods are represented as a thin cylindrical annulus within the row 5 fuel annulus.
- row 7 shim rods are homogenized in with row 7 reflector rods.
- the reactivity worths of row 5 and row 7 rods are adjusted to agree with worths calculated in two-dimensional hexagonal geometry by iteration on the ^{10}B atom densities in the respective annuli.

Doppler coefficients calculated in two dimensions using 2DB[10] and in three dimensions using identical core configurations, densities, and cross sections are given in Table 4.2.1. Corresponding results differ by a maximum of slightly more than 1%.

TABLE 4.2.1
CALCULATED FTR DOPPLER CONSTANTS* Tdk/dt

Temperature Range	Three-Dimensional Method	Two-Dimensional Method
300°K - 1250°K	-.00521	-.00526
1250°K - 2100°K	-.00530	-.00524
300°K - 2100°K	-.00524	-.00526

* The Doppler constants reported here are different from those reported in Reference 9 due to differences in fuel enrichment, loop and test loadings, and control rod configurations.

4.3 BUCKLING CALCULATIONS

Space and energy independent axial buckling, B_Z^2 , is normally inferred from two-dimensional (R,Z) calculations and cylindrical one-dimensional calculations. However, due to the gross heterogeneities present in the FTR and EMC, any two dimensional (R,Z) representation of these cores is somewhat arbitrary. Since different modeling approaches can lead to significantly different results, B_Z^2 values inferred for the FTR and EMC using the usual scheme are uncertain.

Three dimensional calculations presented in this report can be used to infer appropriate buckling values without the inherent modeling problems encountered in the (R,Z) models. The necessary two-dimensional (X,Y) and hexogonal calculations were performed to infer B_Z^2 values for both the FTR and EMC. The three-dimensional calculations which served as a basis for the buckling studies and the inferred bucklings are summarized in Table 4.3.1.

The EMC results indicate that B_Z^2 is not sensitive to the number of energy groups used in the neutronics calculations. For example, if the four group EMC buckling were used in a calculation with 30 group cross sections, the error in the eigenvalue would be approximately 0.0004 Δk.

The results from the two FTR configurations indicate that the axial buckling is sensitive to the row five control rod configuration. With all row five rods inserted the buckling is 0.000590 cm^{-2} whereas with all row five rod withdrawn B_Z^2 is 0.000576 cm^{-2}. Therefore, two-dimensional control rod worth calculations should take into account this buckling change. If this buckling effect were not accounted for in a two-dimensional calculation of the FTR row 5 control rod worth, the calculated rod worth would be~5% low (~0.3% $\Delta K/K$).

TABLE 4.3.1

SUMMARY OF BUCKLING CALCULATIONS

Description	Energy Groups	k_{eff}	B_Z^2 (cm^{-2})
EMC-BOL 3 CR In 3 CR Out 3 PSR In	4	.97838	0.000567
EMC-BOL 3 CR In 3 CR Out 3 PSR In	30	.97868	0.000565
FTR All CR Out 3 PSR In	4	1.01546	0.000576
FTR All CR In 3 PSR In	4	.94531	0.000590

4.4 FTR REACTION RATE DISTRIBUTIONS

Radial fission rates for ^{239}Pu, ^{235}U and ^{238}U near the core midplane were calculated and are shown in Figures 4.4.2 - 4.4.4. Axial fission rate traverses near the core axis for ^{239}Pu and ^{238}U are plotted in Figures 4.4.5 and 4.4.6. Axial ^{10}B (n,α) reaction rates are plotted in Figures 4.4.7 and 4.4.8 for locations near the core axis, through a cocked row 3 safety rod, through a row 3 driver adjacent to a safety rod, and through a row 3 driver away from the safety rod positions. The reaction rates for all processes are normalized to unity at the core center. The direction of the radial traverses and the locations of the axial traverses are identified in Figure 4.4.1 and Table 4.4.1. Also identified on Figure 4.4.1 and Table 4.4.1 are the locations of axial power traces and flux spectra discussed on the following sections.

For ^{239}Pu, the fission rates are calculated using cross section data resonance shielded over the inner driver composition and infinitely delute data. ^{235}U fission rates were computed using inner driver averaged data only. Since ^{238}U fissions occur at energies above the resonance region, the fission cross section of ^{238}U is unaffected by its environment and thus only one set of data need be utilized in computing this fission rate. Also, since ^{10}B has no resonance structure, only one set of data is used in computing ^{10}B (n,α) reaction rates.

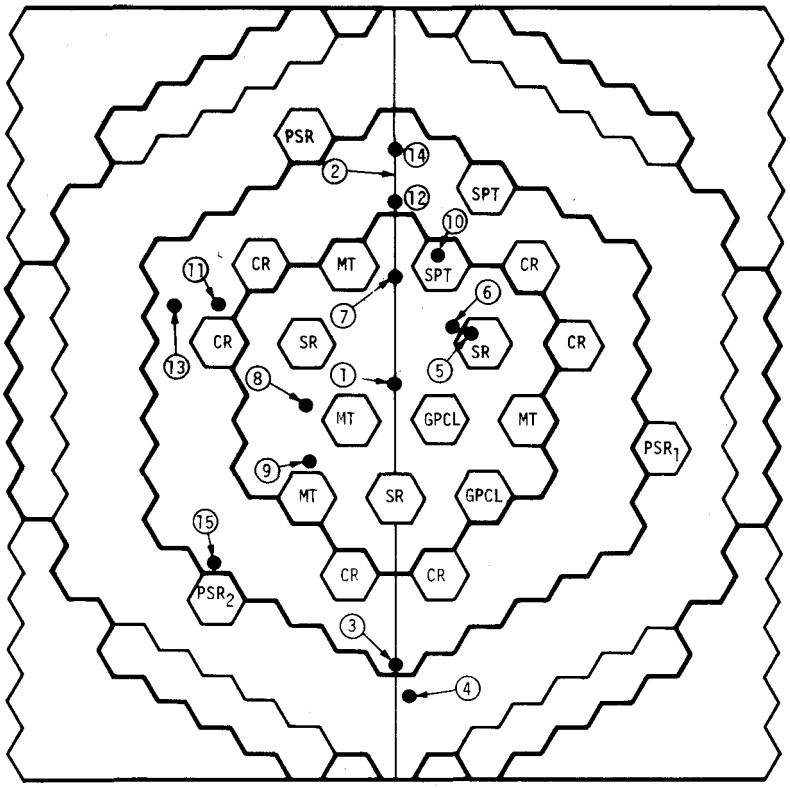

Figure 4.4.1 Locations of FTR reaction rate traverses, power traces and neutron energy spectra (keyed to Table 4.4.1)

TABLE 4.4.1

Identification of Locations of FTR Reaction Rate Traverses, Power Traces and Neutron Energy Spectra

1. Location of "near core axis" axial reaction rate traverses, power traces and neutron energy spectra.
2. Line along which radial reaction rates were plotted.
3. Location of "row 6 driver" spectrum plots.
4. Location of "row 7 driver" spectrum plots.
5. Location of axial B^{10} reaction rate traverses through a cocked safety rod.
6. Location of axial B^{10} reaction rate traverse through a row 3 driver adjacent to a safety rod position.
7. Location of axial B^{10} reaction rate traverse through a row 3 driver distant from the safety rod positions.
8. Locations of axial power trace in a row 3 driver adjacent to a cocked safety rod.
9. Location of axial power trace in a row 3 driver distant from the safety rod positions.
10. Location of axial power trace in row 4 special purpose test.
11. Location of axial power trace in a row 5 driver between two control rods.
12. Location of axial power trace in a row 5 driver distant from the control rod positions.
13. Location of axial power trace in a row 6 driver adjacent to a control rod.
14. Location of axial power trace in a row 6 driver distant from control rods and peripheral shim rods.
15. Location of axial power trace in a row 6 driver near a peripheral shim rod.

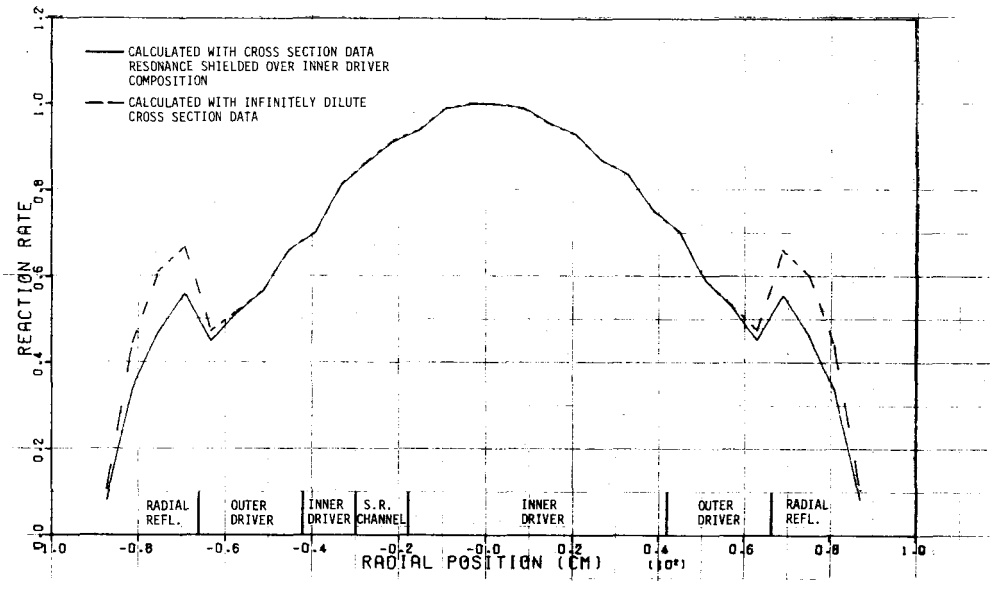

Figure 4.4.2 ^{239}Pu Fission Rate Distribution near Core Midplane of FTR-BOL

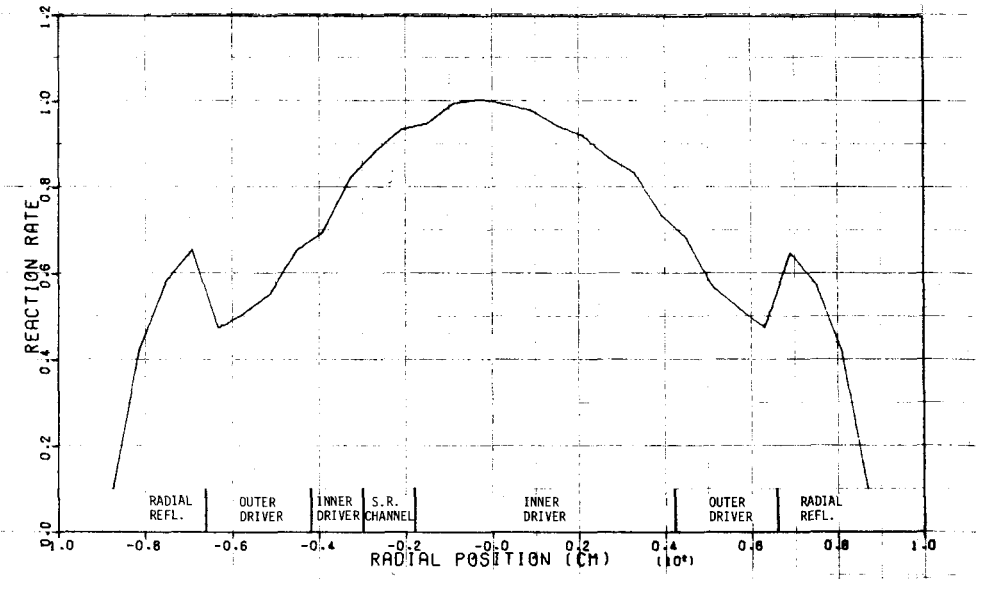

Figure 4.4.3 ^{235}U Radial Fission Rate Distribution near Core Midplane of FTR-BOL

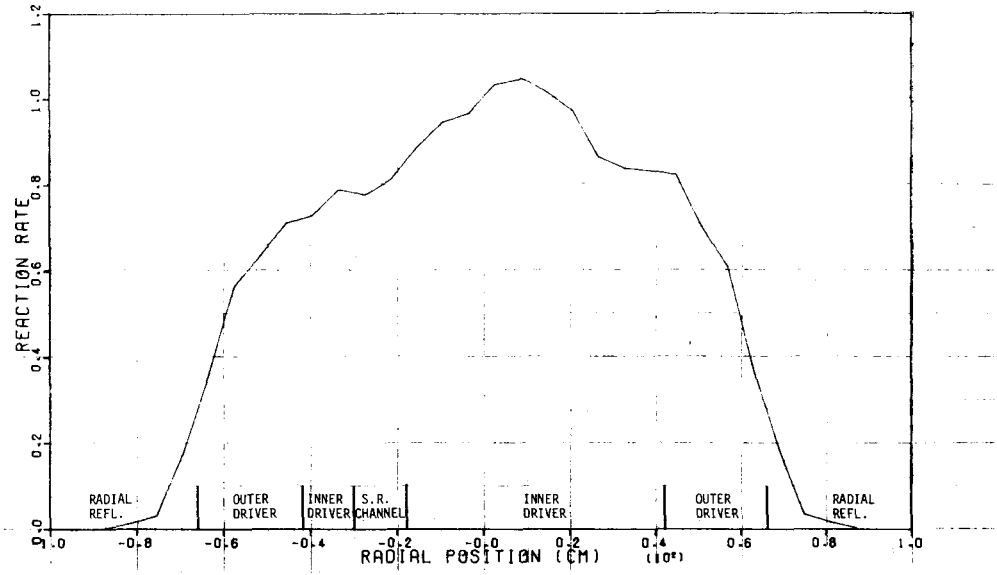

Figure 4.4.4 ^{238}U Radial Fission Rate Distribution near Core Midplane of FTR-BOL

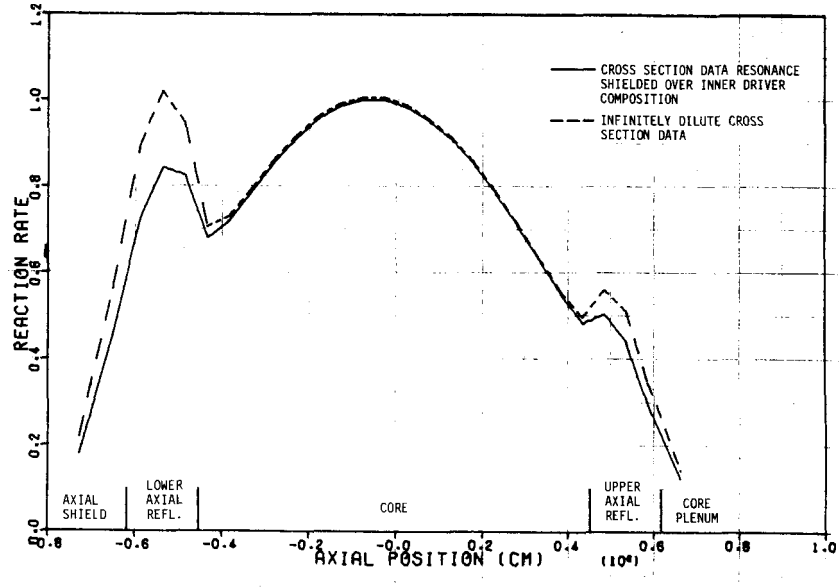

Figure 4.4.5 ^{239} Pu Axial Fission Rate Distribution near Core Axis of FTR-BOL

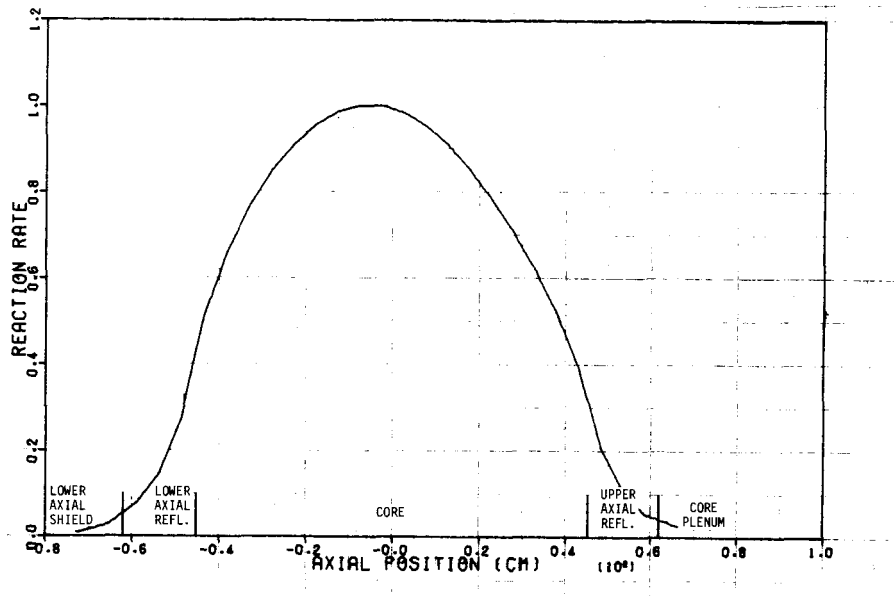

Figure 4.4.6 ^{238}U Axial Fission Rate Distribution near Core Axis of FTR-BOL

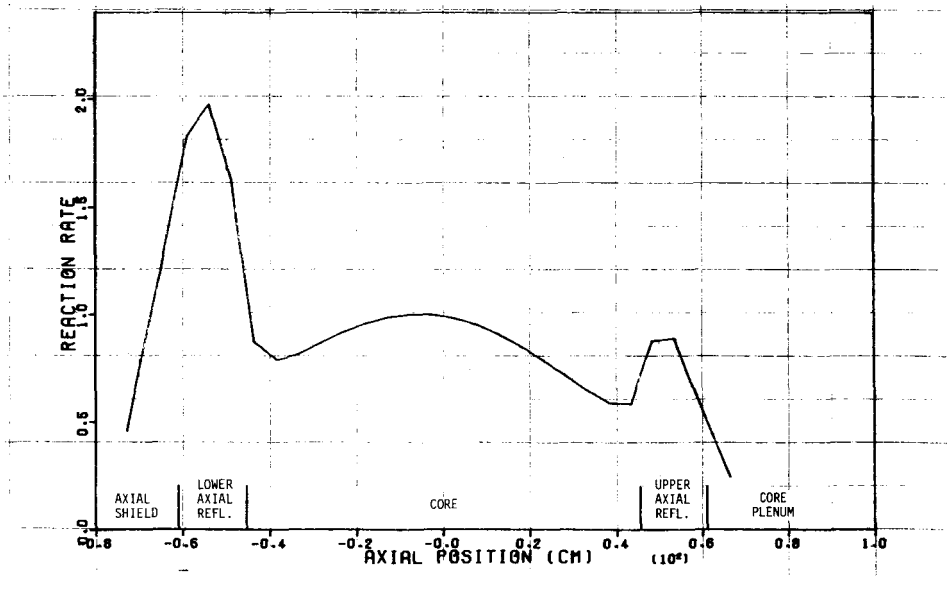

Figure 4.4.7 ^{10}B (n,α) Axial Reaction Rate Distribution near Core Axis of FTR-BOL

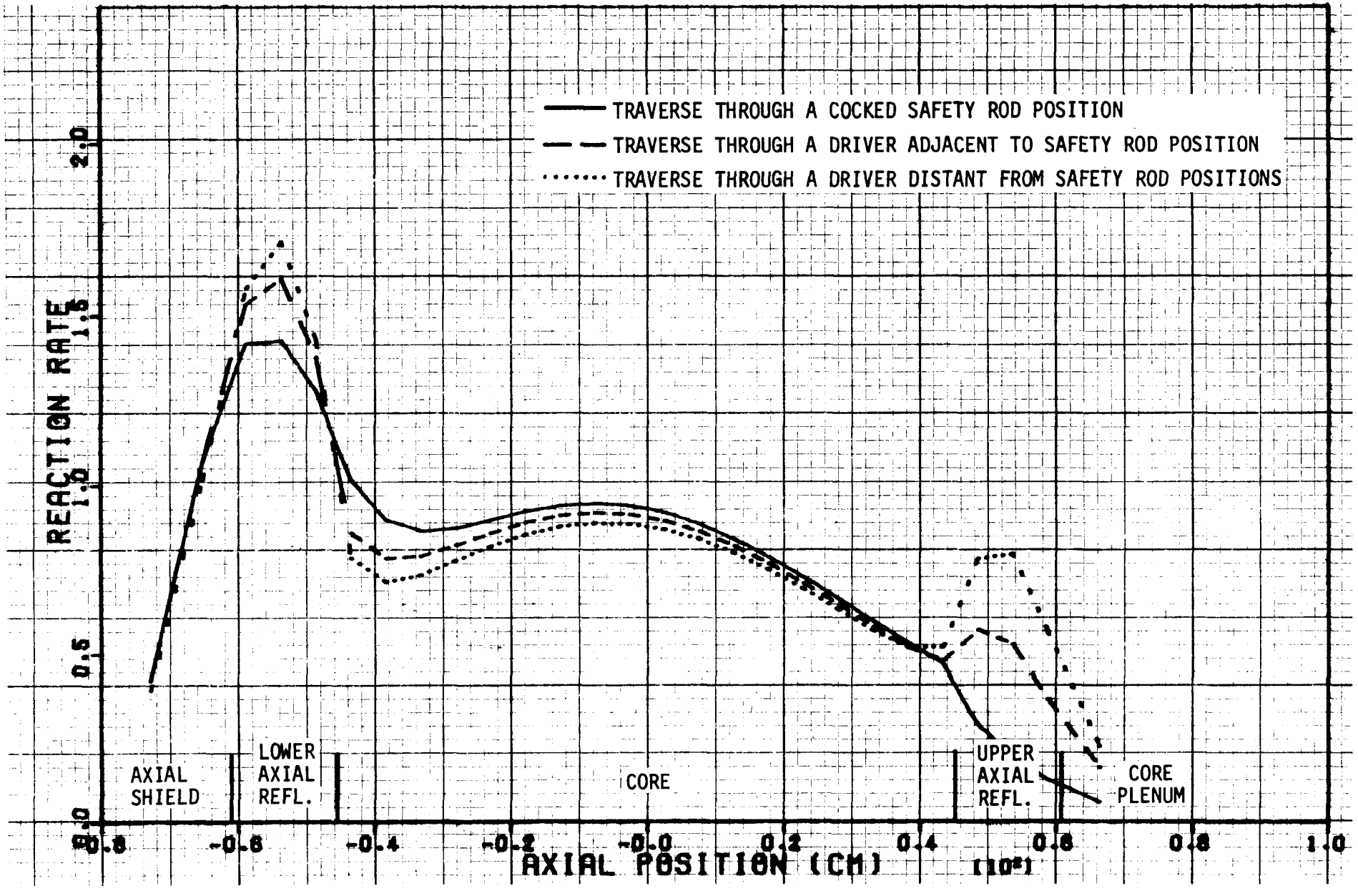

Figure 4.4.8 Comparison of ^{10}B (n,α) Axial Reaction Rate Distribution in Row 3 Locations of FTR-BOL

4.5 CALCULATED POWER DISTRIBUTION IN THE FTR-BOL

In the 3DB calculations of the FTR-BOL, the model employed contained 27 inner driver subassemblies, 47 outer driver subassemblies, 2 general purpose closed loops, and 2 special purpose test positions. The power produced on each of these 78 fueled positions is shown in Figure 4.5.1, with the total power produced in the core normalized to 400 megawatts. The peak to average power (power factor) in each of these 78 subassemblies is shown in Figure 4.5.2 and the axial power factor for each radial mesh point is shown in Figure 4.5.3.

Axial power traces at selected radial locations are shown in Figures 4.5.4-4.5.8. The positions are identified in Figure 4.4.1 and Table 4.4.1. They include locations near the core axis, in row 3 drivers adjacent to and distant from safety rod positions, in the row 4 special purpose test loop, in a row 5 driver between two control rods, in a row 5 driver away from the control rods, in row 6 drivers adjacent to and distant from the control rods and in a row 6 driver adjacent to a peripheral shim rod. In Figures 4.5.7 and 4.5.8, the depressions in the axial power profiles near the partially inserted row 5 control rods can be seen. All the power traces indicated that the power is axially skewed everywhere in the core due to the effects of the partially inserted control rods and the cocked safety rods. Also from these plots and Figure 4.5.3, it is clear that the axial power peaking is greatest near the partially inserted control rods and least near the core axis and the loop positions.

Radial power factors for each axial plane in the core are listed in Figure 4.5.1. In computing these, all drivers plus the four lightly fueled loop positions were included. The radial power factors range in value from 1.34 at the core bottom monotonically increasing to 1.51 near the top of the core. The core midplane value is 1.39 and the overall power factor in the FTR-BOL is 1.73.

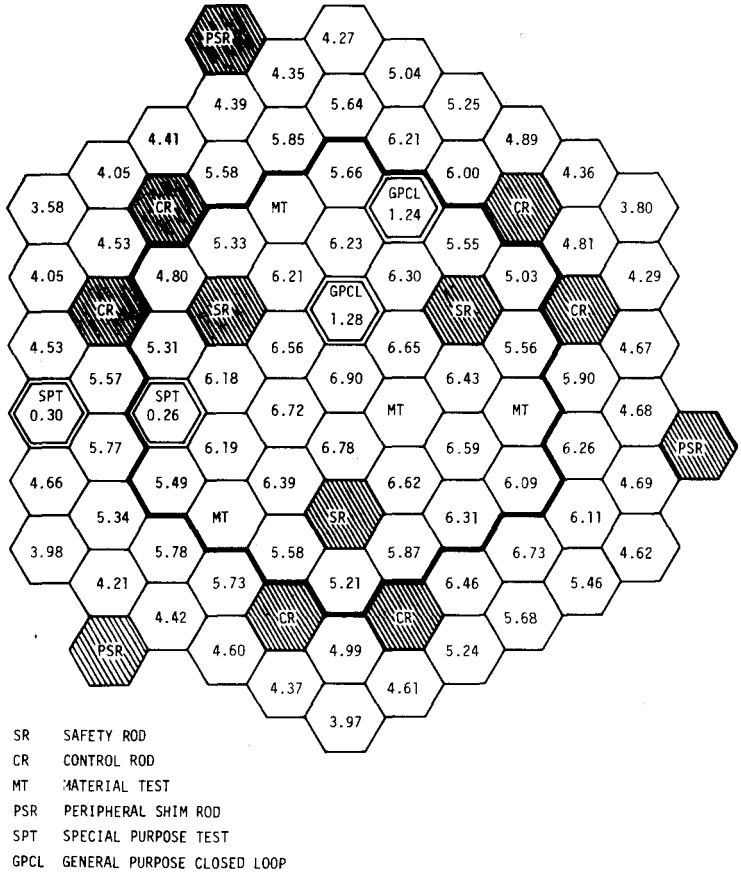

Figure 4.5.1 Total Power Produced Per Subassembly in FTR-BOL (Mw)

TABLE 4.5.1

RADIAL (BY PLANE) AND OVERALL FTR POWER FACTORS

Plane (K)	Average Power Density (mW/ℓ)	Peak Power Density (mW/ℓ)	Peak Location (I, J, K)	Power Factor
6	.3728	.4993	25 15 6	1.339
7	.4035	.5328	15 15 7	1.320
8	.4445	.5934	15 14 8	1.335
9	.4834	.6516	15 14 9	1.348
10	.5159	.6999	15 14 10	1.357
11	.5400	.7363	15 14 11	1.363
12	.5548	.7597	15 14 12	1.369
13	.5596	.7699	15 14 13	1.376
14	.5542	.7669	15 14 14	1.384
15	.5385	.7512	15 14 15	1.395
16	.5123	.7238	15 14 16	1.413
17	.4808	.6861	15 14 17	1.427
18	.4455	.6396	15 14 18	1.436
19	.4065	.5855	15 14 19	1.440
20	.3643	.5250	15 14 20	1.441
21	.3199	.4639	25 15 21	1.450
22	.2750	.4046	25 15 22	1.471
23	.2351	.3541	25 15 23	1.506
OVER ALL	.4448	.7699	15 14 13	1.731

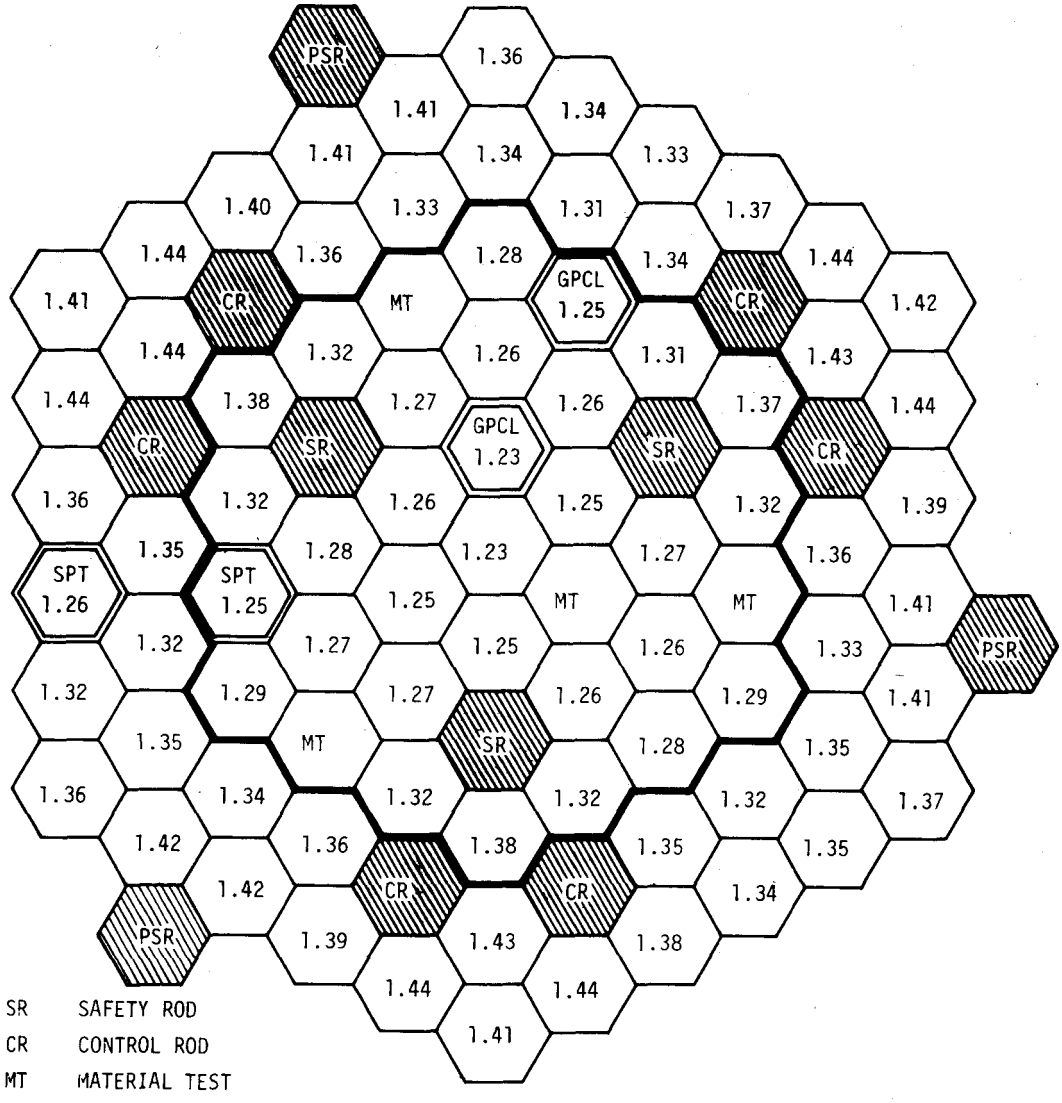

SR SAFETY ROD
CR CONTROL ROD
MT MATERIAL TEST
PSR PERIPHERAL SHIM ROD
SPT SPECIAL PURPOSE TEST
GPCL GENERAL PURPOSE CLOSED LOOP

Figure 4.5.2 Peak to Average Power per Subassembly in FTR-BOL

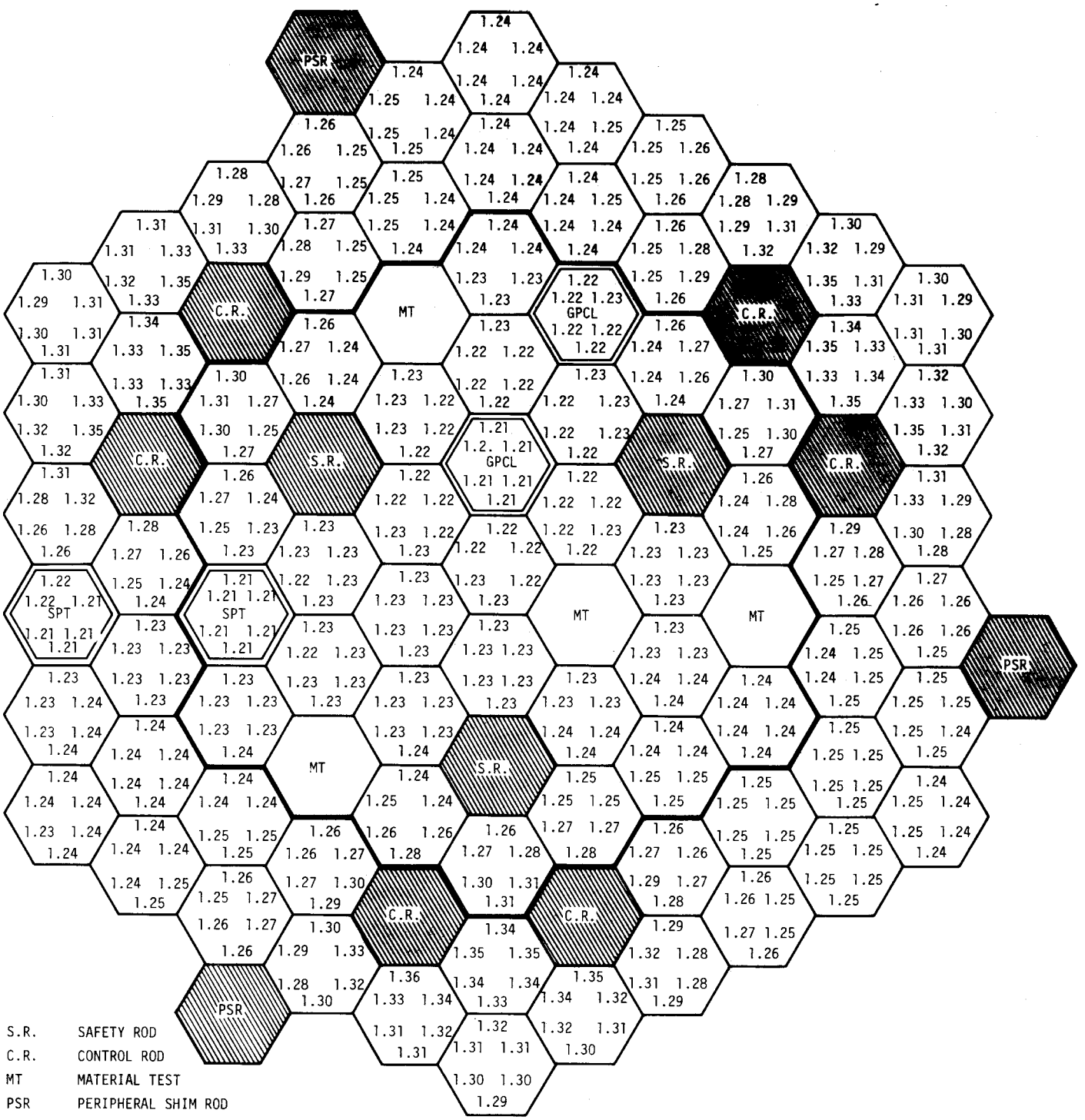

Figure 4.5.3 Axial Power Peaking Factor at Each Radial Mesh Point in the FTR-BOL

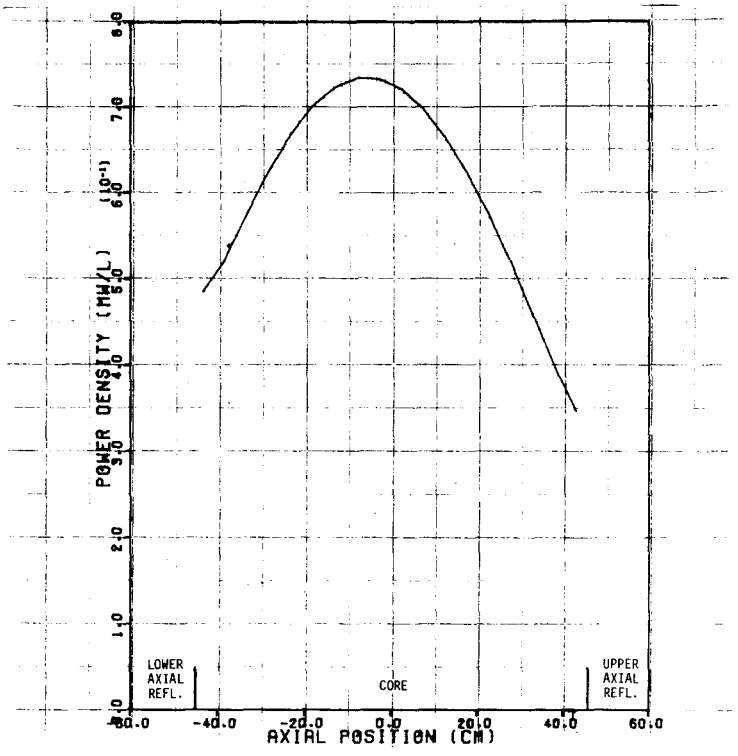

Figure 4.5.4 Axial Power Profile near Core Axis of FTR-BOL

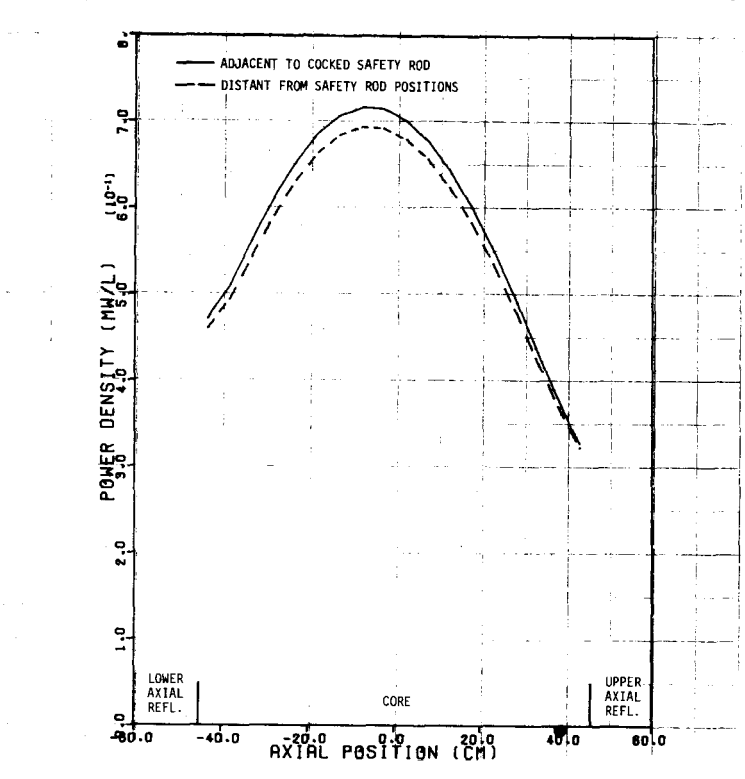

Figure 4.5.5 Axial Power Profile in Row 3 Drivers of FTR-BOL

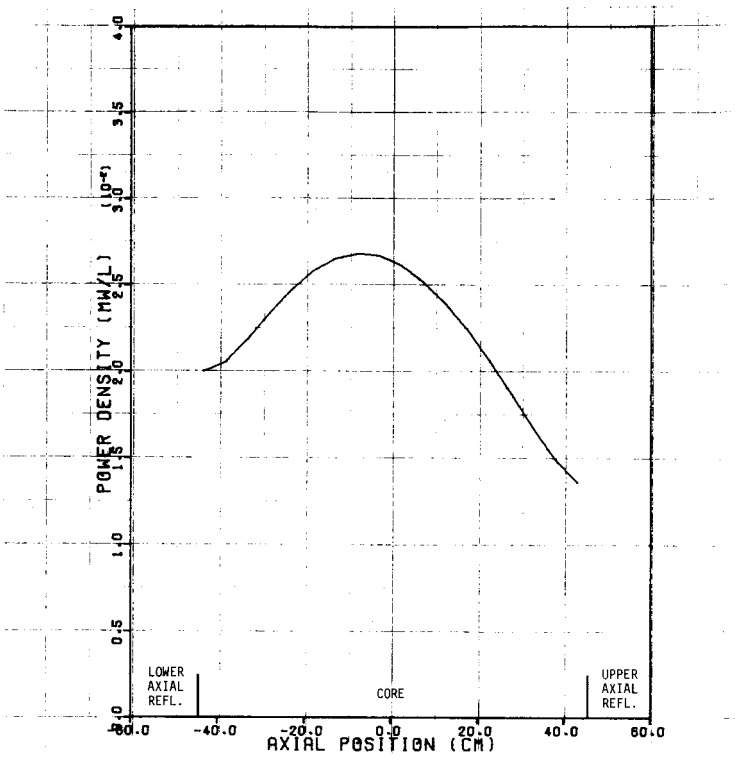

Figure 4.5.6 Axial Power Profile in the Row 4 Special Purpose Tes'

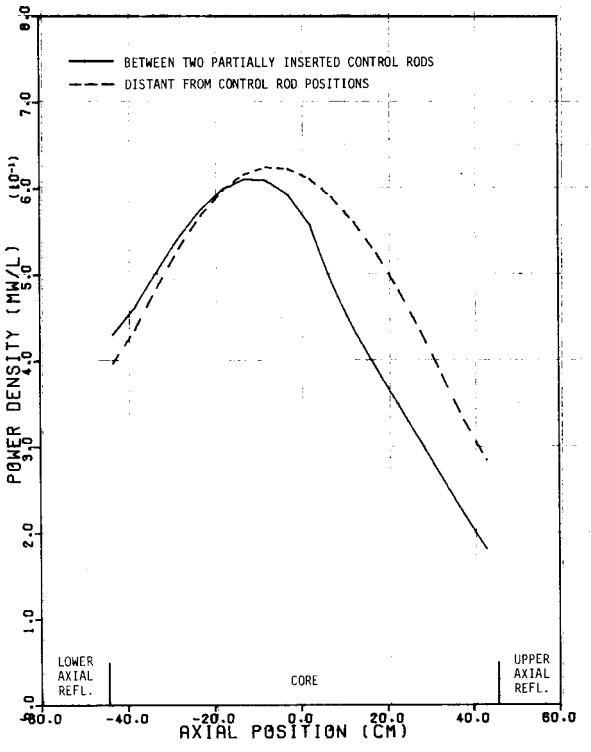

Figure 4.5.7 Axial Power Profiles in Row 5 Drivers of FTR-BOL

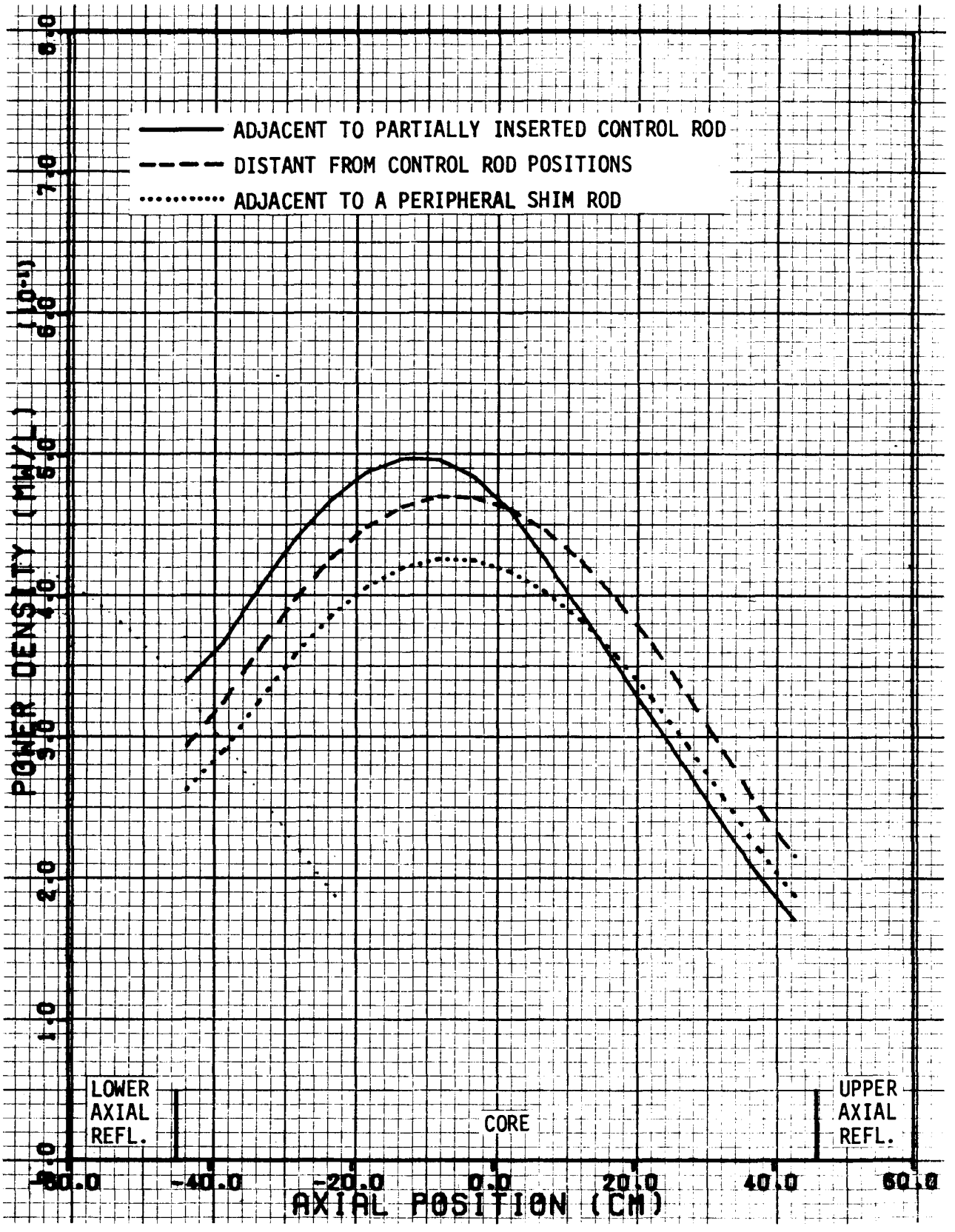

Figure 4.5.8 Axial Power Profiles in Row 6 Drivers of FTR-BOL

4.6 FTR NEUTRON ENERGY SPECTRA

Flux spectra from the final FTR-BOL 30 group calculation are shown in Figures 4.6.1-4.6.8. The six space points for which spectra are plotted are located radially near the core center, in a row 6 driver assembly, and in a row 7 reflector assembly, as shown in Figure 4.4.1, and axially near the reactor midplane and near the top of the core. Differential flux spectra for the three locations near the reactor midplane are shown in Figures 4.6.1 - 4.6.3. The integrated flux spectra for these locations are compared in Figure 4.6.4. The corresponding spectra plotted for the locations near the top of the core are shown in Figures 4.6.5 - 4.6.8.

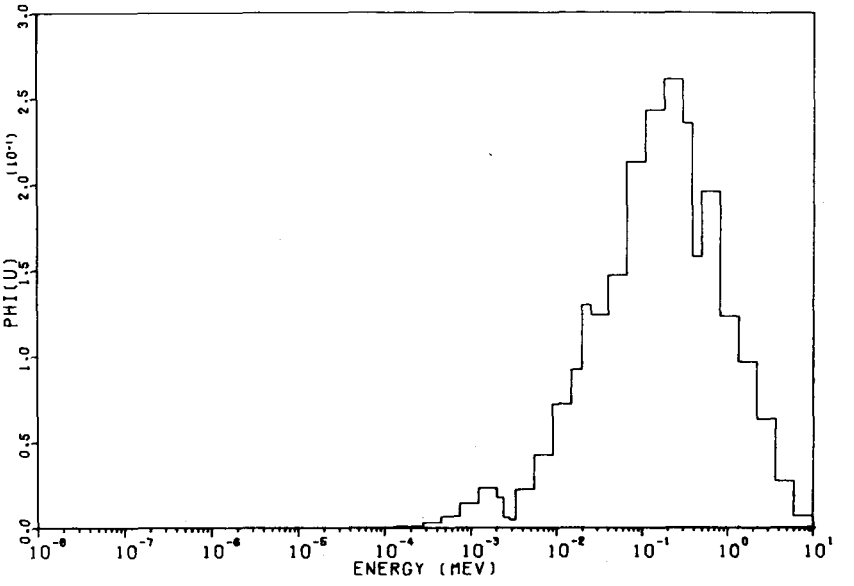

Figure 4.6.1 FTR-BOL 30 Group Neutron Energy Spectrum near the Core Center.

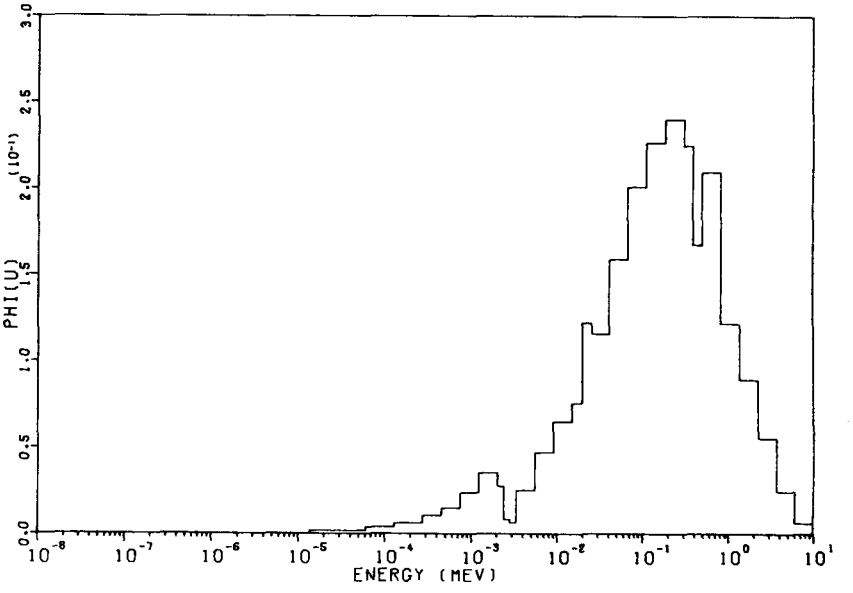

Figure 4.6.2 FTR-BOL 30 Group Neutron Energy Spectrum at edge of Row 6 Driver at Core Midplane.

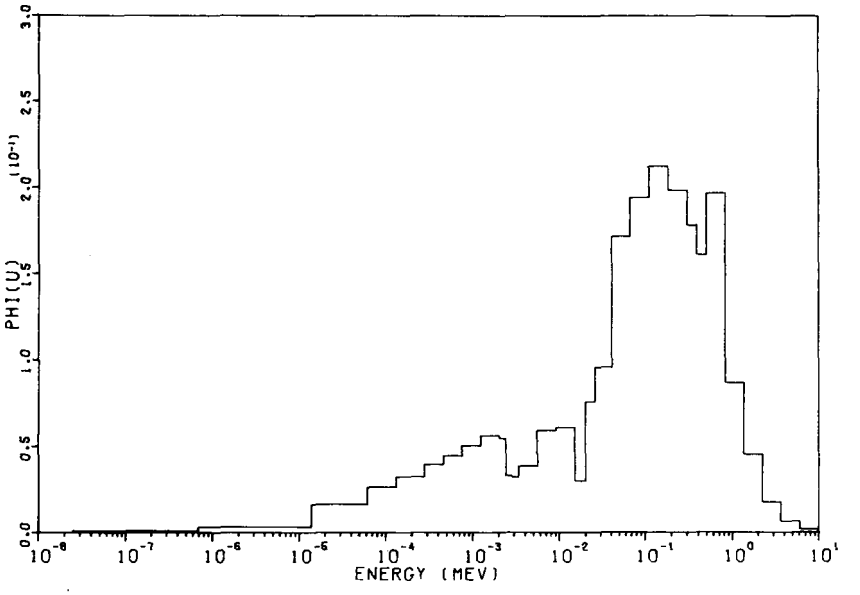

Figure 4.6.3 FTR-BOL 30 Group Neutron Energy Spectrum in Row 7 Reflector Assembly at Core Midplane.

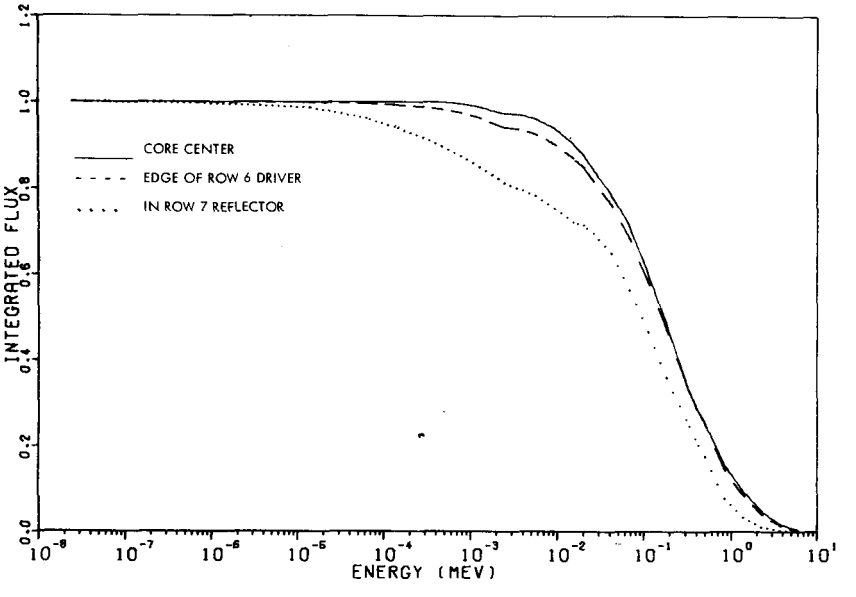

Figure 4.6.4 Comparison of FTR-BOL Integrated Neutron Energy Spectra at the Core Midplane.

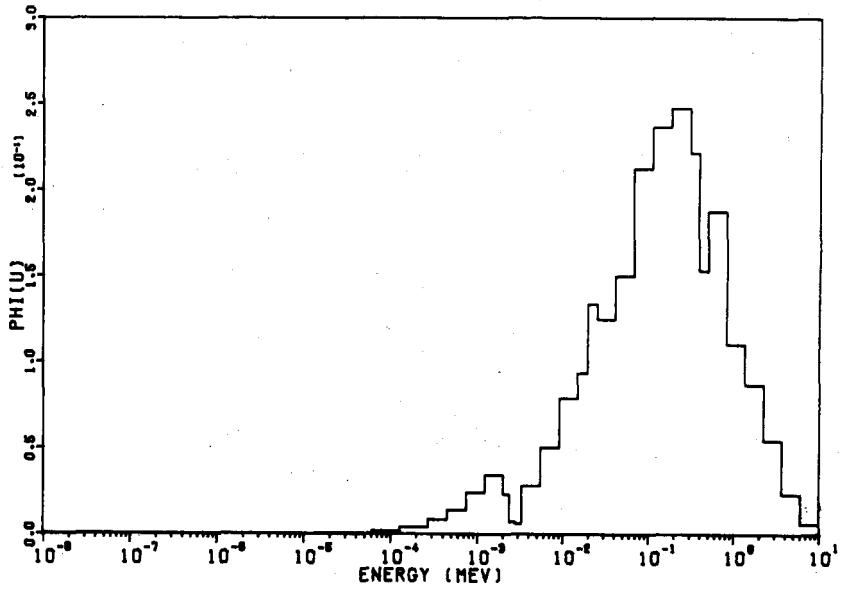

Figure 4.6.5 FTR-BOL 30 Group Neutron Energy Spectrum near the Core Axis at Top of Core.

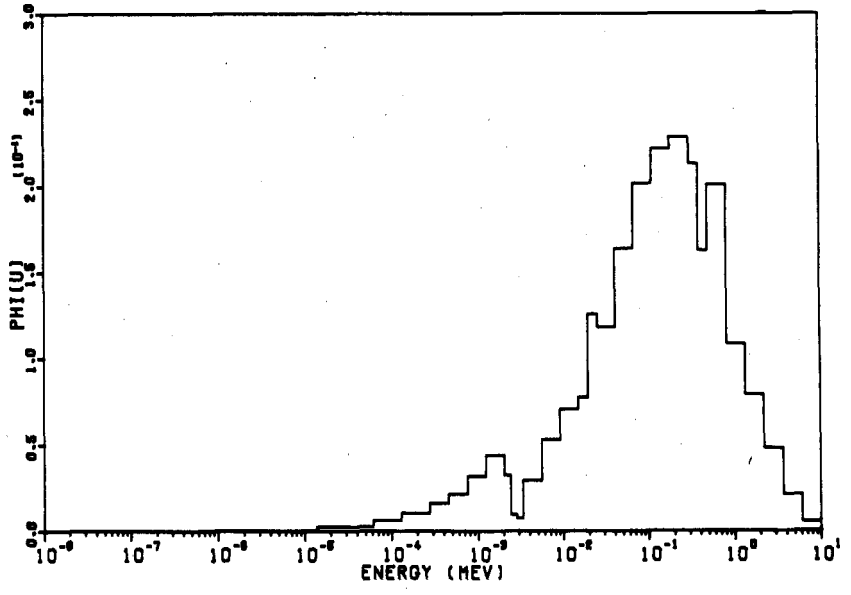

Figure 4.6.6 FTR-BOL Group Neutron Energy Spectrum in Row 6 Driver at Top of Core.

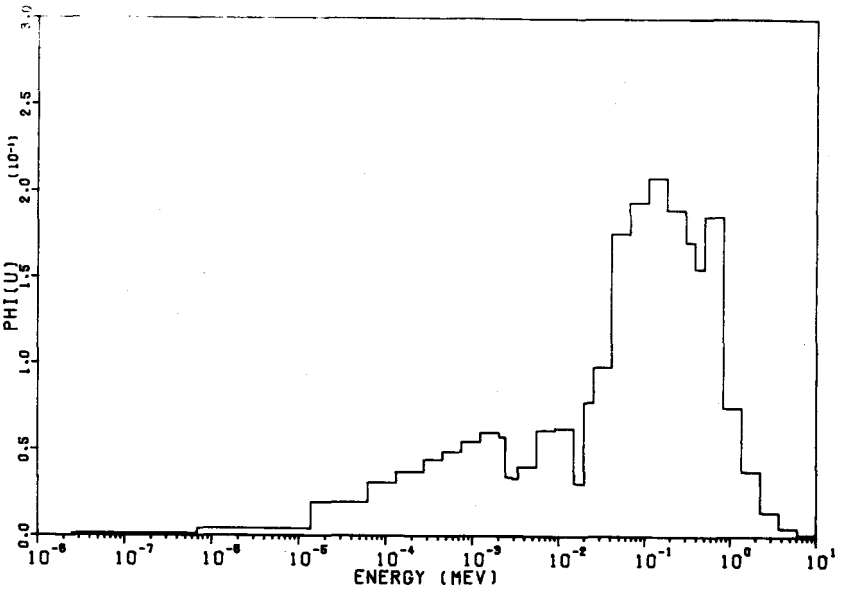

Figure 4.6.7 FTR-BOL 30 Group Neutron Energy Spectrum in Row 7 Reflector Assembly at Top of Core.

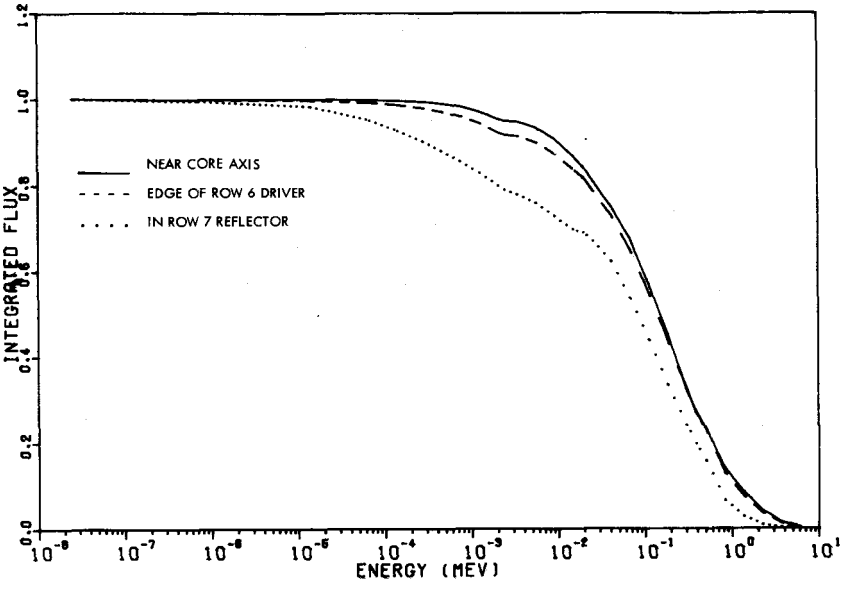

Figure 4.6.8 Comparison of FTR-BOL Integrated Neutron Energy Spectra at Locations near Top of Core.

REFERENCES

1. Hardie, R. W. and Little, W. W., Jr., "3DB A Three-Dimensional Diffusion Theory Burnup Code", BNWL-1264, Battelle Northwest, Richland, Washington, 1970.

2. Schenter, R. E., Kidman, R. B. and Nelson, J. V., "FTR Set 300, Multigroup Cross Sections for FTR Design", HEDL-TME 71-153, WADCO Corporation, Richland, Washington, 1971.

3. Hardie, R. W. and Little, W. W., Jr., "IDX, A One-Dimensional Diffusion Code for Generating Effective Nuclear Cross Sections", BNWL-954, Battelle Northwest, Richland, Washington, 1969.

4. Ramchandran, S. and Madden, G. H., unpublished data (ARD-FRP-518).

5. Reactor Development Program Progress Report, ANL 7854, Argonne National Laboratory, Argonne, Illinois, August 1971.

6. ANL-FFTF Critical Experiments Program Monthly Informal Technial Progress Report Argonne National Laboratory, December 1971 - January 1972 (unpublished).

7. Reactor Development Program Progress Report, ANL 7758, Argonne National Laboratory, Argonne, Illinois, November 1970.

8. Nelson, J. V. (unpublished data).

9. Baloh, F., and Ramchandran, S., unpublished data (ARD-FRP-619).

10. Little, W. W., Jr., and Hardie, R. W., "2DB User's Manual--Revision 1", BNWL-831 Rev. 1., Battelle Northwest, Richland, Washington, 1969.

11. ANL-FFTF Critical Experiments Program Monthly Informal Technical Progress Report, Argonne National Laboratory, February 1971, (unpublished).

12. Calamai, George J., unpublished data, (ARD-FRP-568).

13. Little, W. W., Jr., private communication.

APPENDIX A
CROSS SECTION PREPARATION

Cross sections used in the three dimensional calculations were taken from the FTR design set 300[2] and resonance self shielded in the one dimensional cross section preparation program IDX[3]. EMC cross sections were homogeneously resonance self-shielded whereas FTR cross sections were heterogenously resonance self-shielded through use of the Bell correction option in IDX.

Calculations for both assemblies were performed using both 30 and 4 group cross section libraries. Four group cross sections were created by collapsing thirty group cross sections in IDX. Group one of the four group sets was collapsed from the first seven groups of the 30 group set; group two from groups 8-12 of the 30 group set; group three from groups 13-17 of the 30 group set; and group four from the remaining 13 groups.

Figures A-1 and A-2 depict the cylindrical (r) model used for core radial reflector, and control rod cross section preparation and the slab (Z) model used for axial reflector cross section preparation, respectively. The zones described for the cylindrical model were defined such that FTR volume and mass were conserved. These dimensions were also used for EMC cross section preparation. Material mixtures contained in the various zones of Figures A-1 and A-2 are described in Table A-1. Table A-II gives the details of the resonance self-shielding and callapsing operations performed in IDX. Cross sections for the Engineering Mockup were resonance self-shielded at room temperature. Cross sections for FTR were resonance self shielded at hot temperatures, i.e., fuel at 1250°K and diluent at 750°K. For the purpose of Doppler calculations, FTR 30 group cross sections were also resonance self-shielded, with the U-238 isotope temperature at 300°K and 2100°K.

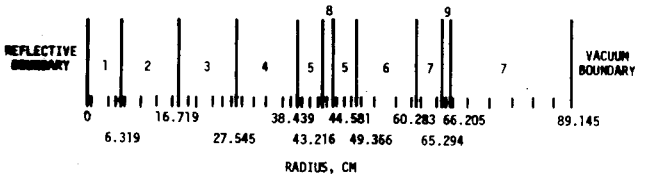

Figure A-1 Cylindrical IDX Model

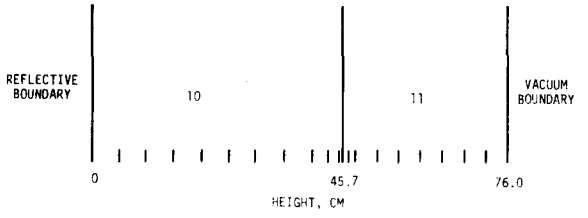

Figure A-2 Slab IDX Model

TABLE A-1

IDX ZONE COMPOSITION

Zone	FTR	EMC
1	100% Inner Driver	100% Inner Driver
2	66.7% Inner Driver 16.7% General Purpose Loop 16.7% Material Test	67.4% Inner Driver 16.3% General Purpose Loop 16.3% Sodium Channel
3	75% Inner Driver 25% Sodium Channel	75.6% Inner Driver 24.4% Sodium Channel
4	72.2% Inner Driver 11.1% General Purpose Loop 16.7% Material Test	73.0% Inner Driver 10.8% General Purpose Loop 16.2% Material Test
5	85.7% Outer Driver 14.3% Sodium Channel	86.2% Outer Driver 13.8% Sodium Channel
6	96.7% Outer Driver 3.3% General Purpose Loop	96.8% Outer Driver 3.2% General Purpose Loop
7	100% Radial Reflector	100% Radial Reflector
8	100% Control Rod	100% Control Rod
9	100% Peripheral Shim Rod	100% Peripheral Shim Rod
10	100% Inner Driver	100% Inner Driver
11	100% Axial Reflector	100% Axial Reflector

TABLE A-2

CROSS SECTION PREPARATION DETAILS

	Resonance Self-Shielding Composition in Zone From Figs. A-1 and A-2	Cross Sections Collapsed In Spectrum from Zone In Figures A-1 and A-2
INNER DRIVER	1	2
OUTER DRIVER	6	6
CONTROL ROD	5	8
RADIAL REFLECTOR	7	7
PERIPHERAL SHIM ROD	5	9
AXIAL REFLECTOR	11	11

APPENDIX B
EMC 3DB MODEL DESCRIPTION

All mixtures used in EMC calculations are identified by number in Table B-1. Figures B-1 through B-7 describe by number and zone the composition of the seven axial layers of the EMC 3DB model. Slight simplifications were made in the geometric model in order to minimize the required number of axial layers. The modifications are small and considered insignificant. They may be studied by comparing the attached figures, Figures 3.1.1 and 3.1.2 in the main text, and the as built EMC configuration as reported by Argonne National Laboratory[11].

TABLE B-1
EMC MIXTURE IDENTIFICATION

Mixture Number	Mixture
35	Inner Driver
36	Outer Driver
37	Sodium Channel
38	General Purpose Loop
39	Special Purpose Loop
40	Control Rod
41	Peripheral Shim Rod
42	Radial Reflector
43	Oscillator Poison Section
44	Axial Reflector
45	Control Rod Shield
46	Handling Socket
47	Drive Shaft
48	Material Test
49	Core Plenum
50	Control Rod Plenum
51	Axial Shield
52	Radial Reflector Shield
53	ZPR-9 Stainless Steel Mixture

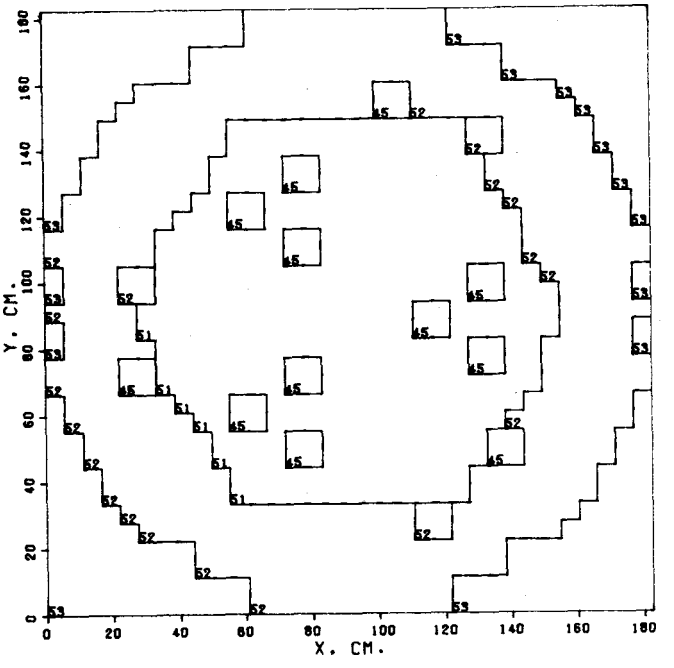

Figure B-1 EMC Layer 1 - Lower Axial Shield Region

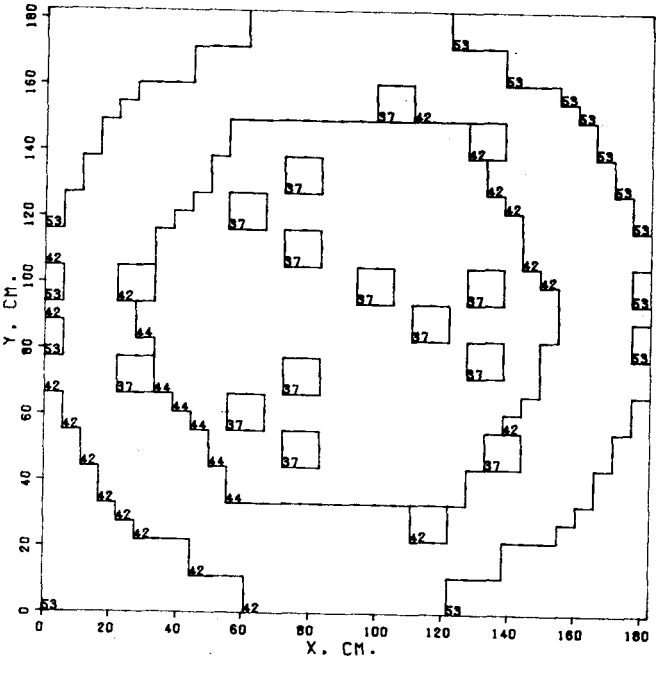

Figure B-2 EMC Layer 2 - Lower Axial Reflector Region

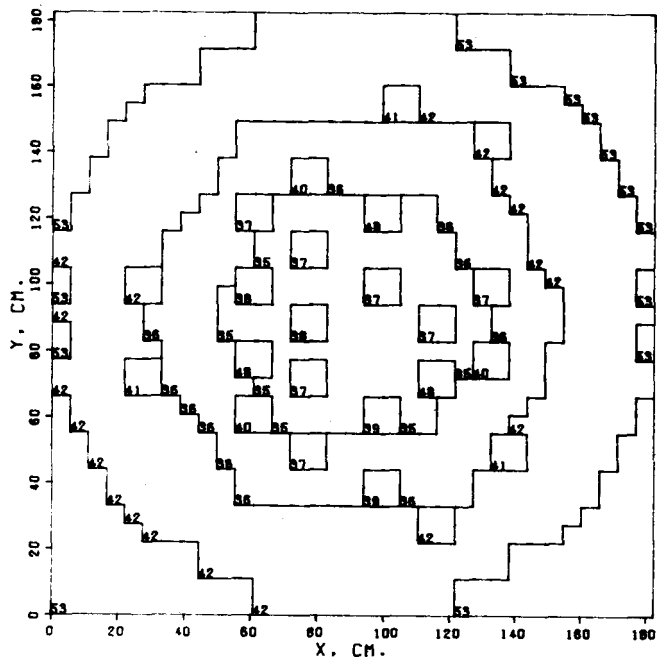

Figure B-3 EMC Layer 3 - Lower Core Region

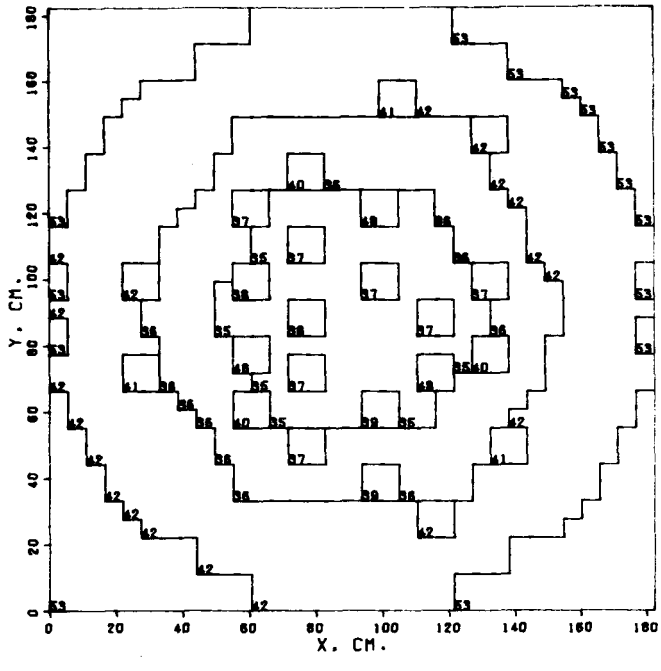

Figure B-4 EMC Layer 4 - Upper Core Region

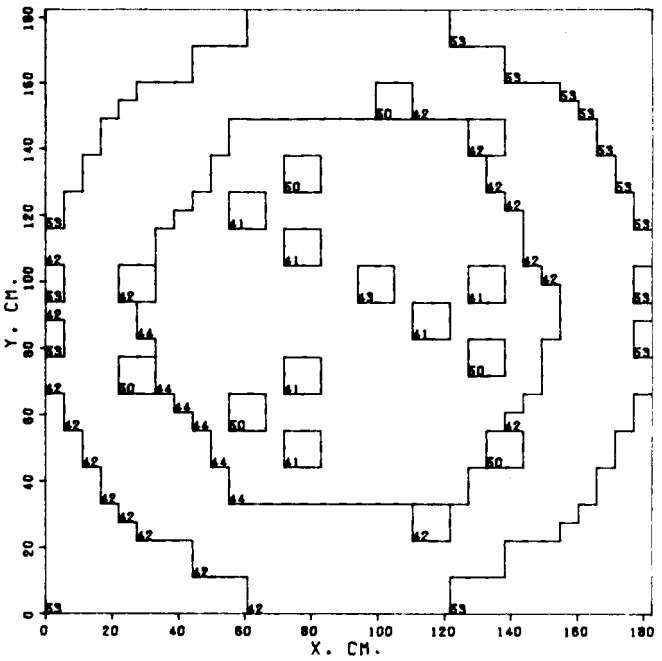

Figure B-5 EMC Layer 5 - Upper Axial Reflector Region

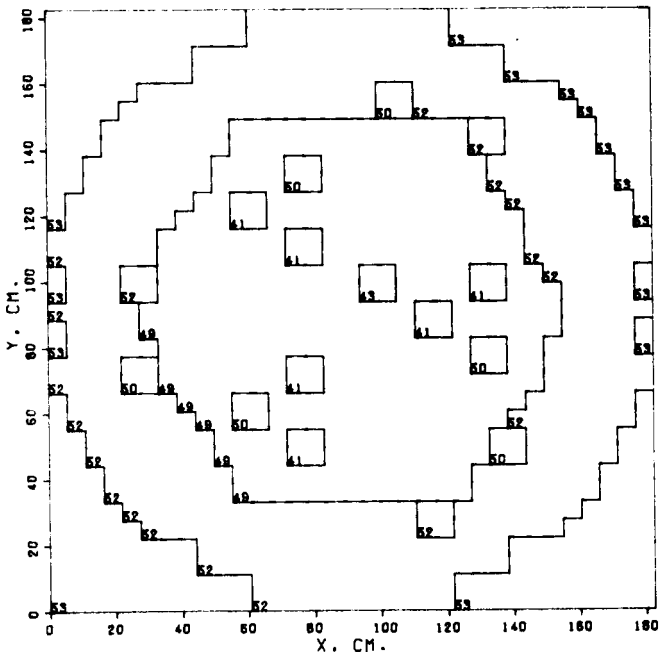

Figure B-6 EMC Layer 6 - Plenum Region

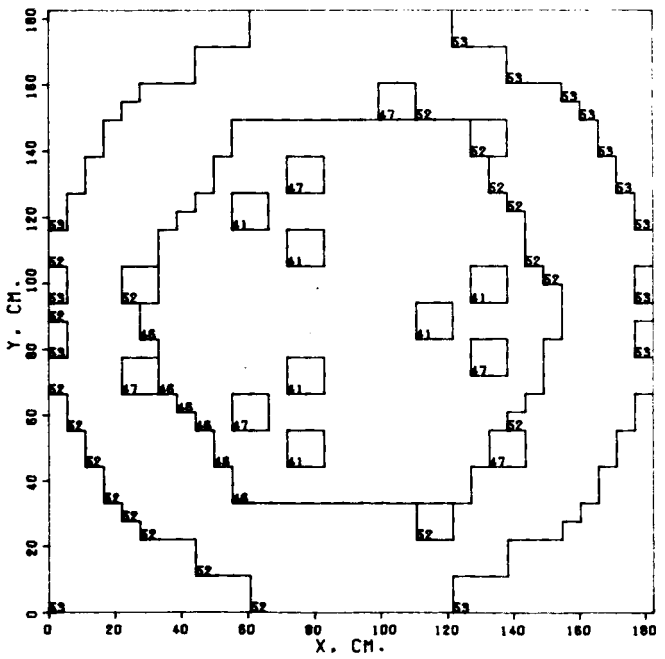

Figure B-7 EMC Layer 7 - Handling Socket Region

APPENDIX C
FTR 3DB MODEL DESCRIPTION

Atom densities used for FTR-3DB calculations are listed in Table C-1 and compared to the most recent FTR densities [12]. All mixtures used in FTR calculations are identified by number in Table C-2. Figures C-1 through C-7 describe by number and zone the composition of all seven layers of the 3DB model having all rods inserted 16 inches into the core. For clarity, Figures C-1 through C-7 may be compared to Figures 4.1.1 and 4.1.2 of the main text.

Figures C-8, through C-11 compare the axial definition achieved in the 3DB model with the current FTR design for driver, control rod, safety rod and reflector assemblies respectively. The notable differences were necessary in order to fit the model into the available computer small core memory and are estimated to have little effect on the core neutronic parameter of interest. Listed in Table C-3 are atom densities of mixtures which were omitted from the 3DB Model. These may be compared with densities given in Table C-1.

TABLE C-1

FTR ATOM DENSITIES (10^{21} atom/cm^3)

	Inner Driver			Outer Driver		
	N_1*	N_2**	N_0***	N_1	N_2	N_0
^{239}Pu	1.4112	1.3982	1.3686	1.6595	1.7039	1.6786
^{240}Pu	.1924	.1898	.1879	.2263	.2328	.2302
^{241}Pu	.00	.0027	.0264	.000	.0033	.0324
^{235}U	.0392	.0403	.0397	.0372	.0377	.0372
^{238}U	5.5577	5.7168	5.6319	5.2868	5.3604	5.2808
0	14.2017	14.4744	14.2913	14.2273	14.4805	14.3007
Na	8.9561	8.9651	9.0950	8.9561	8.9561	9.0950
S/S	19.8199	19.8199	19.5714	19.8199	19.8199	19.5714

	General Purpose Loop-Row 2/Row 4		Special Purpose Loop - Row 4/Row 6	
	N_1	N_0	N_1	N_0
^{239}Pu	.2380	.2382	.0451	.0451
^{240}Pu	.0325	.0325	.0451	.0061
^{241}Pu	.000	.000	.000	.0000
^{235}U	.0484/.0683	.0384/.0684	.0230/.0511	.0231/.0511
^{238}U	.9203/.8903	.9209/.8910	.1583/.1302	.1584/.1303
0	2.4217	2.424	.4582	.4585
Na	15.7246	14.444	17.1523	15.7569
S/St	18.6004	18.6136	17.3043	17.3166

TABLE C-I (CONT)

	Radial Reflector		Upper Axial Reflector		Lower Axial Reflector		Sodium Channel	
	N_1	N_0	N_1	N_0	N_1	N_0	N_1	N_0
Na	2.1824	2.084	8.9441	9.0828	8.9682	9.1073	19.7142	20.1620
S/S	1.9541	11.8891	19.7934	19.5450	19.8466	19.5977	7.9386	7.9041
Inc+	77.1966	66.9221	28.9236	27.8855	29.0069	27.9606		

	Material Test		Radial Shield		Axial Shield	
	N_1	N_0	N_1	N_0	N_1	N_0
Na	9.098	9.1463	1.1908	4.4192	5.2108	5.666
S/S	47.347	46.8331	77.6881	63.8868	63.2668	61.2939

	Control Rod		Control Plenum		Core Plenum	
	N_1	N_0	N_1	N_0	N_1	N_0
Na	6.9223	7.1653	7.1680	7.1162	8.9441	9.0102
S/S	24.7828	23.8685	23.6530	31.3454	19.7934	24.1807
C	9.1024	9.1500				
10B	7.2849	7.3206				
11B	29.1275	29.2823				

FOOTNOTES TO TABLE C-1

*	N_1	Concentrations used in calculations 4 through 6, as listed in Appendix D.
**	N_2	Concentrations used in calculations 7 through 13, as listed in Appendix D, if different from N_1.
***	N_0	Current design concentrations.

+SS =	$67.2^{Wt}/0$	Fe
	$18.05^{Wt}/0$	CR
	$11.29^{Wt}/0$	Ni
	$3.45^{Wt}/0$	Mo
+Inc	$7.4^{Wt}/0$	Fe
	$17.43^{Wt}/0$	Cr
	$74.55^{Wt}/0$	Ni
	$0.21^{Wt}/0$	Mo
	$0.41^{Wt}/0$	Si

TABLE C-2

FTR MIXTURE IDENTIFICATION

Mixture Number	Mixture
35	Inner Driver
36	Outer Driver
37	Row - 2 General Purpose Loop
38	Row - 4 General Purpose Loop
39	Row - 4 Special Purpose Loop
40	Row - 6 Special Purpose Loop
41	Sodium Channel
42	Control Rod
43	Peripheral Shim Rod
44	Material Test
45	Radial Reflector (Rows 7 and 8)
46	Radial Reflector (Row 9)
47	Lower Axial Reflector
48	Upper Axial Reflector
49	Radial Shield
50	Axial Shield
51	Core Plenum
52	Control Rod Plenum

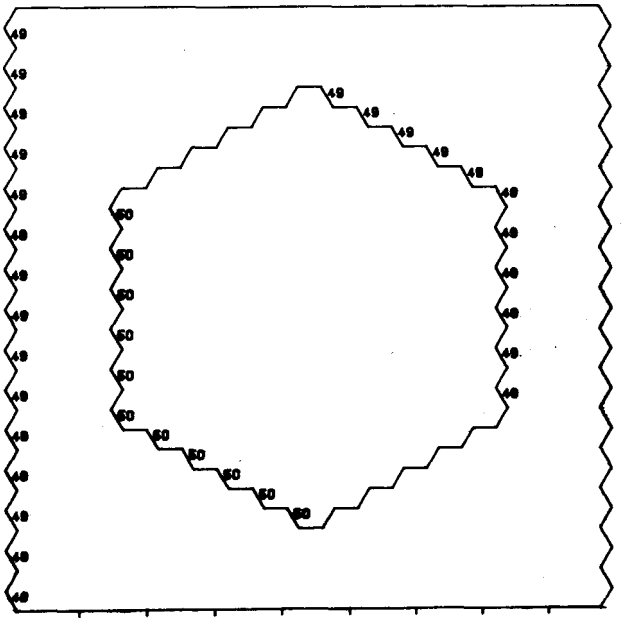

Figure C-1 FTR Layer 1 - Lower Axial Shield Region

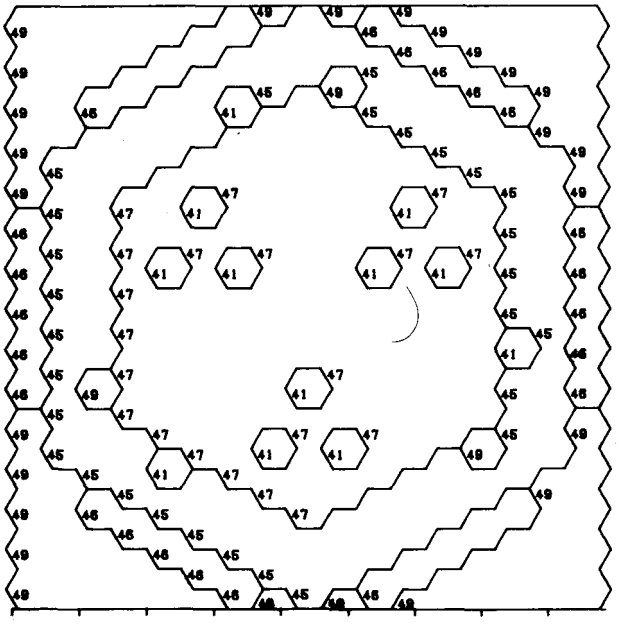

Figure C-2 FTR Layer 2 - Lower Axial Reflector Region

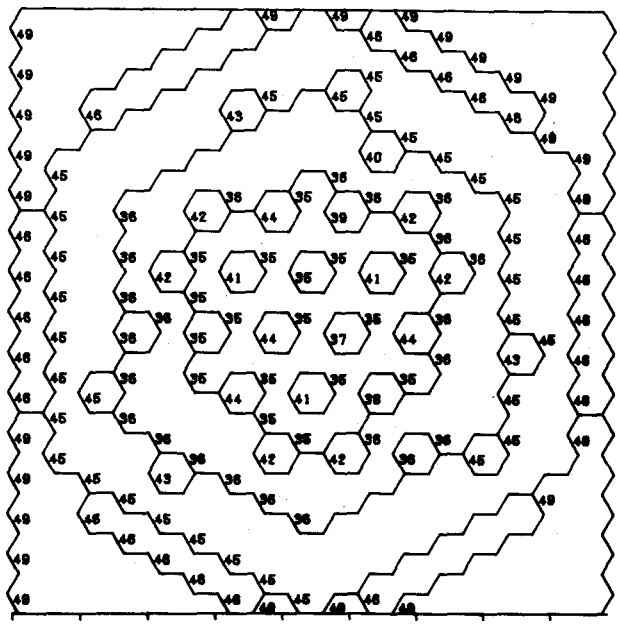

Figure C-3 FTR Layer 3 - First Core Layer

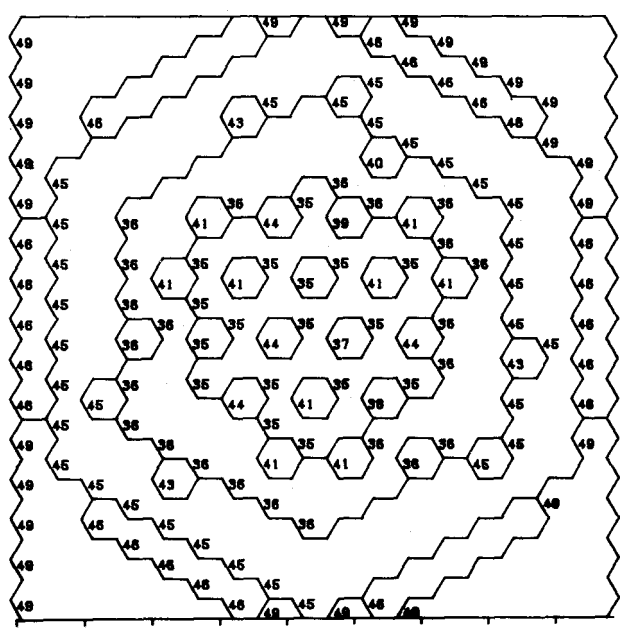

Figure C-4 FTR Layer 4 - Second Core Layer

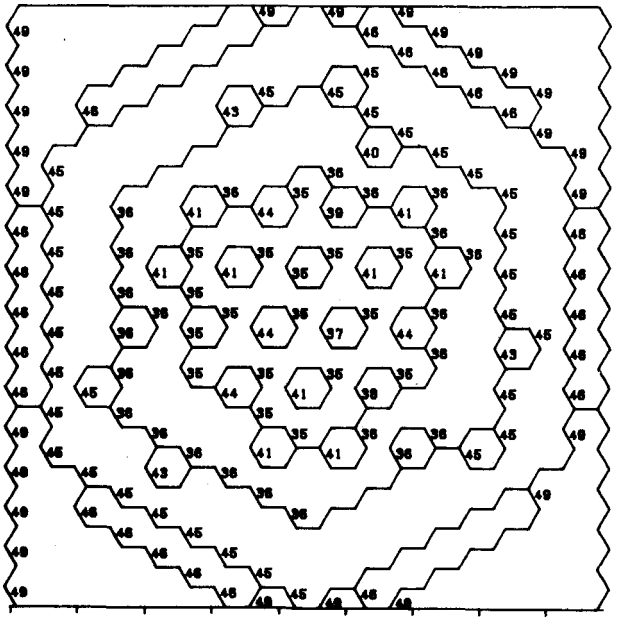

Figure C-5 FTR Layer 5 - Third Core Layer

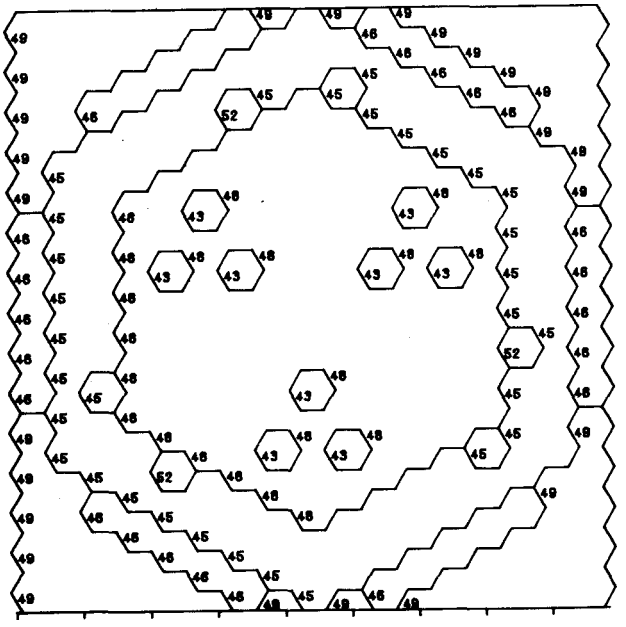

Figure C-6 FTR Layer 6 - Upper Axial Reflector Region

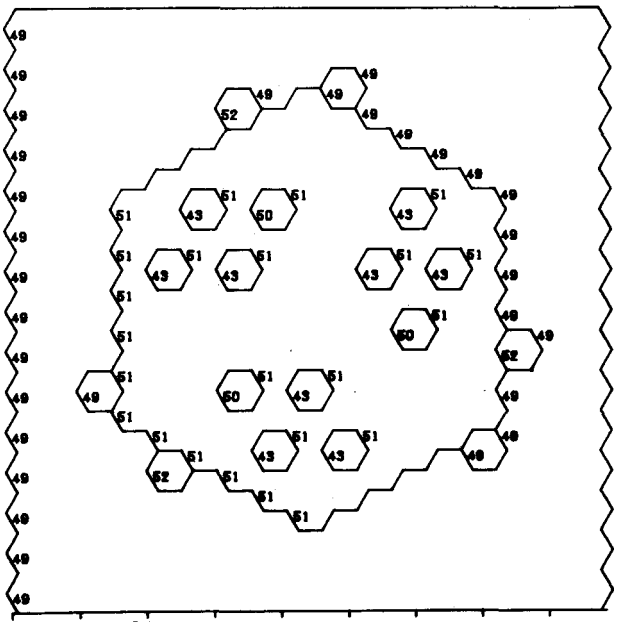

Figure C-7 FTR Layer 7 - Core Plenum Region

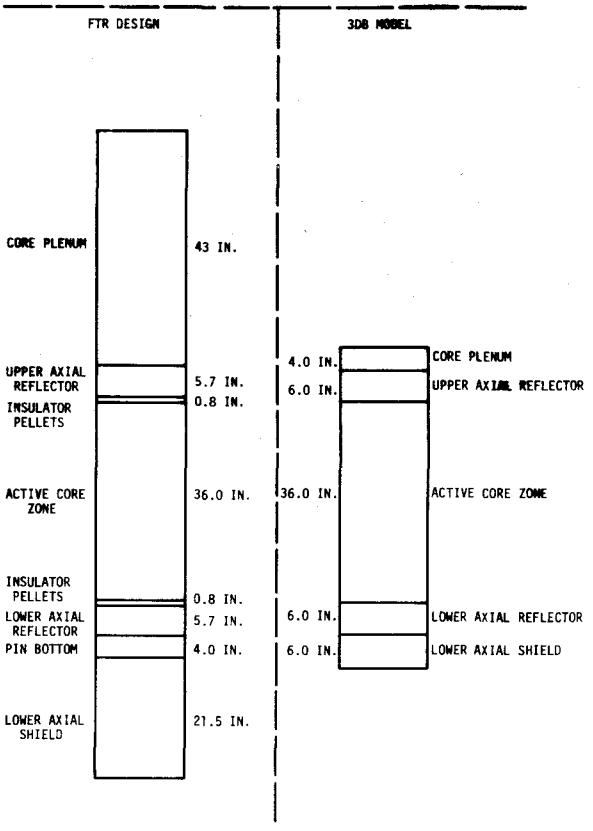

Figure C-8 Comparison of 3DB Model Driver Assembly with current FTR Design

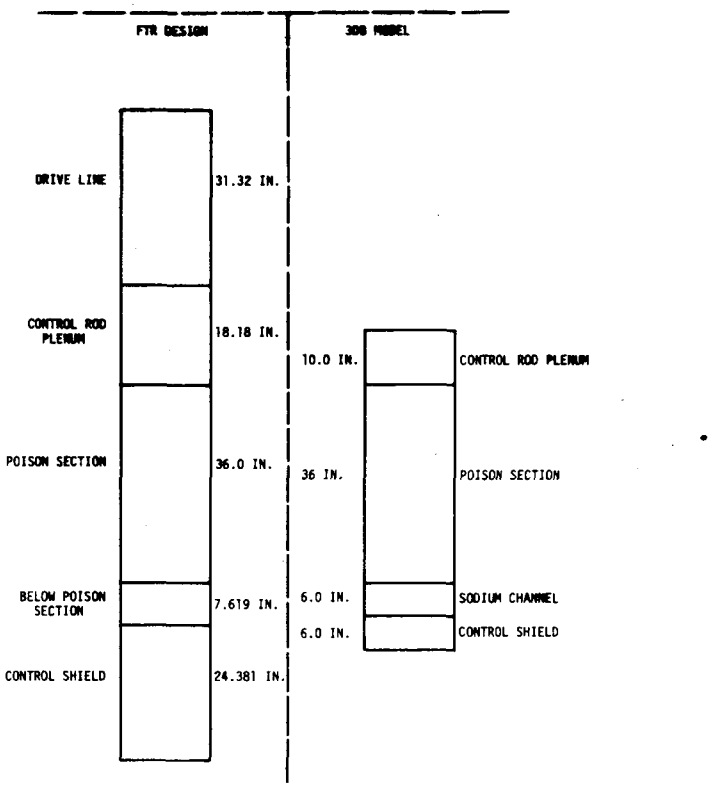

Figure C-9 Comparison of 3DB Model Fully Inserted Control Rod with Current FTR Design

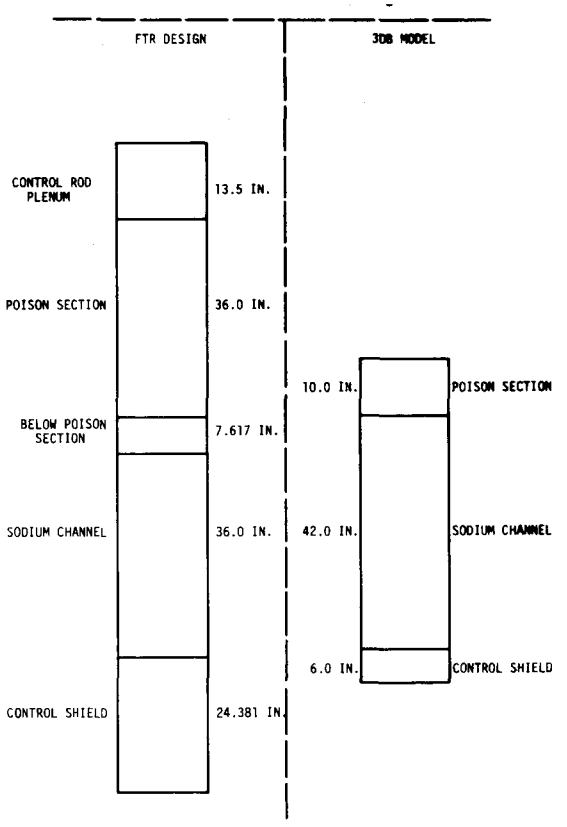

Figure C-10 Comparison of 3DB Model Fully Withdrawn Control Rod with Current FTR Design

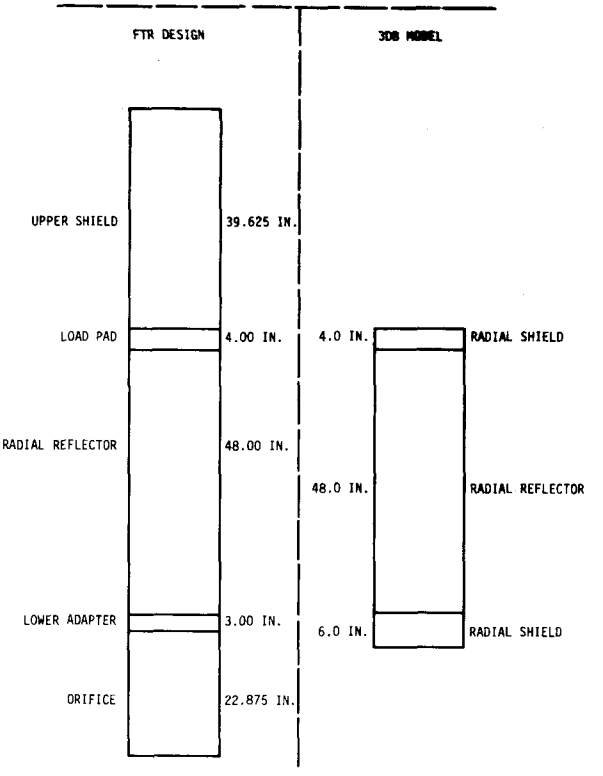

Figure C-11 Comparison of 3DB Model Reflector Assembly with current FTR Design

TABLE C-3

MATERIAL ATOM DENSITIES FOR WHICH SUBSTITUTIONS WERE MADE IN 3DB (10^{21} at/cm^3)

	Insulator Pellet	ID Pin Bottom	OD Pin Bottom	Below Poison Section
Na	9.0950	13.0078	13.2086	13.3938
S/S	19.57136	34.25312	33.51447	32.8324
^{238}U	7.2666			
^{235}U	0.0512			
0	14.41608			

	Orfice	Lower Adapter	Load Pad
Na	5.1576	4.3255	1.5192
S/S	63.1672	66.3206	76.5680

APPENDIX D
3DB CONVERGENCE BEHAVIOR

The convergence time of 3DB is a strong function of the initial flux guess. A summary of all 3DB runs discussed in this report is given in Table D-1. The overall convergence behavior of the runs is described in Figure D-1 and D-2. Figure D-2 is a blow-up of the more interesting features of Figure D-1. Individual curves are labeled with numbers which correspond to run numbers given in Table D-1. Some curves have been translated on the eigenvalue scale for the convenience of plotting.

In general the convergence behavior is quite uniform after the first few iterations. A striking exception is observed in run No. 4 where the eigenvalue converged to 2.7×10^{-5} and then turned around to coverage at a lower value. However, in this case the total Δk change in the last nine iterations was only 0.00015.

It is difficult to tell from Figures D-1 and D-2 whether, in fact, the eigenvalue is sufficiently converged or just what the converged eigenvalue would be. The latter is more easily shown by plotting the information in a different fashion. Figure D-3 displays eigenvalues (once again translated for convenience) plotted against $1 - \lambda$ where λ is the 3DB convergence indicator. The nearly linear nature of the data suggests a straight forward technique for extrapolating to the best eigenvalue estimate. This has been done for all runs which had a sufficient number of iterations for extrapolation, and the extrapolated values are noted in Table D-1. Whenever available, extrapolated eigenvalues have been used throughout the main text of this report.

All 30 group calculations were performed in runs of two outer iterations each. At the end of each run the fluxes were written to tape and used to start the next set of two iterations. In Figure D-4 the convergence behavior of the 30 group EMC run (No. 2) is displayed. This figure is comparable with the continuous 4 group runs in Figure D-3. The striking difference is most likely due to the restart mode of calculations in the 30 group run. 3DB uses a convergence acceleration scheme for both the flux and fission source distribution which involves both the current and previous values. When a problem is restarted, this acceleration scheme cannot be employed on the fission source since the previous fission source distribution is no longer available.[13] The lack of fission source acceleration accounts for the strange convergence behavior in Figure D-4 and most likely attenuates the convergence. The magnitude of this attenuation has not been quantitatively assessed but it is estimated to be small.

It was determined that by essentially expanding a four group flux dump to 30 groups and using that as a flux start for the 30 group problem, substantial time could be saved. This was done for the initial FTR-30 group calculation (No. 9) but not for the EMC 30 group calculation. The computer time savings is conservatively estimated at ~60 min. for the 30 group FTR calculation.

TABLE D-1

SUMMARY OF 3DB RUNS

	Description	σ'S	Flux Start	K (Eigenvalue)	λ (Convergence)	Extrapolated Eigenvalue	Time
1.	EMC-3 Rods In 3 Rods Out 3 PSR In	4 Groups	SHAPE*	0.97825	1.000044	.97838	35.8 min.
2.	EMC-3 Rods In 3 Rods Out 3 PSR In	30 Groups Homogeneous	SHAPE*	0.97853	1.00007	.97868	205.8 min.
3.	FTR All Rods Out 3 PSAR In Old Enrichment	4 Groups Bell Corrected	FROM PREVIOUS 4 Group Run	1.01548	.9999909	1.01546	25.3 min.
4.	FTR All Rods @18 inches 3 PSR In Old Enrichment	4 Groups Bell Corrected	FROM PREVIOUS 4 Group Run	0.98086	.9999905	.98083	23.8 min.
5.	FTR All Rods In 3 PSR In Old Enrichment, 1250°K	4 Groups Bell Corrected	FROM PREVIOUS 4 Group Run	0.94531	1.000007	.94532	25.7 min.
6.	FTR All Rods @16 inches 3 PSR In Old Enrichment	4 Groups Bell Corrected	FROM RUN No. 5	0.98678	.9999908	.98675	27.7 min.
7.	FTR All Rods @16 inches 3 PSR In New Enrichment, 1250°K	4 Groups Bell Corrected	FROM RUN No. 6	0.98981	.9999908	.9898	16.3 min.
8.	FTR 5 Rods @16 inches 1 Rod @18 inches 3 PSR In New Enrichment, 1250°K	4 Groups Bell Corrected	FROM RUN No. 7	0.98877	.9999968		5.2 min.
9.	FTR 5 Rods @16 inches 1 Rod @18 inches 3 PSR In New Enrichment, 1250°K	30 Groups Bell Corrected	RUN No. 6***	0.9879	.999953		79.7 min.

TABLE D-1 (Cont'd)

Description	σ'S	Flux Start	K (Eigenvalue)	λ (Convergence)	Extrapolated Eigenvalue	Time
10. FTR 6 Rods @ 16 inches 3 PSR In New Enrichment 1250°K	30 Groups Bell Corrected	RUN No. 9	0.98885	1.000041		26.6 min.
11. FTR 6 Rods @16 inches 3 PSR In New Enrichment U-238 @ 2100°K	30 Groups Bell Corrected	RUN No. 10	0.99629	1.000002		50.6 min.
12. FTR 6 Rods @16 inches 3 PSR In New Enrichment U-238 @2100°K	30 Groups Bell Corrected	RUN No. 10	0.98610	1.000027		25.9 min.
13. FTR-Burnup 5 Rods @16 inches 1 Rod @18 inches 3 PSR In, New Enrichment BURN FOR TEN DAYS	4 Groups Bell Corrected	RUN No. 8	0.98584	0.9999965		8.3 min.

---

* START FLUX:

$$\phi(R) = 1.0 - \frac{|R|}{B_R + a}$$

where R is either X, Y or Z and R=O at core center. B_R is the distance from the core center to the boundary of the problem in dimension R and $B_R + a$ is the special position at which the flux is zero. a is adjusted so that $\phi(B_R)$ is approximately 0.01.

*** Fluxes from 4 group run were expanded to thirty groups by setting the first seven groups of the thirty group fluxes equal to group one of the four group fluxes, groups 8-12 equal to group 2, groups 13-17 equal to group 3, and groups 18-30 equal to group 4.

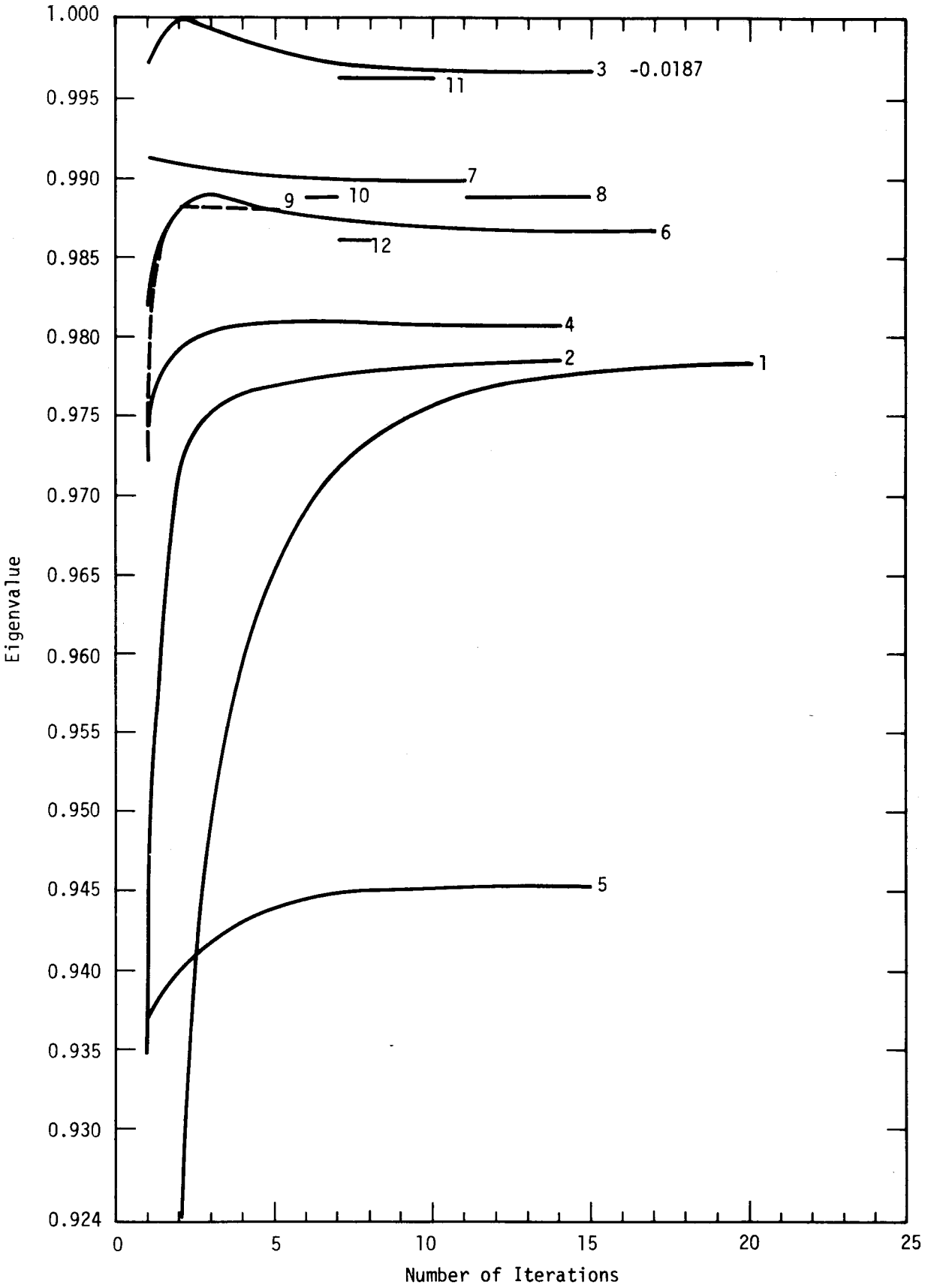

Figure D-1 Gross Convergence Behavior of all 3DB Calculations

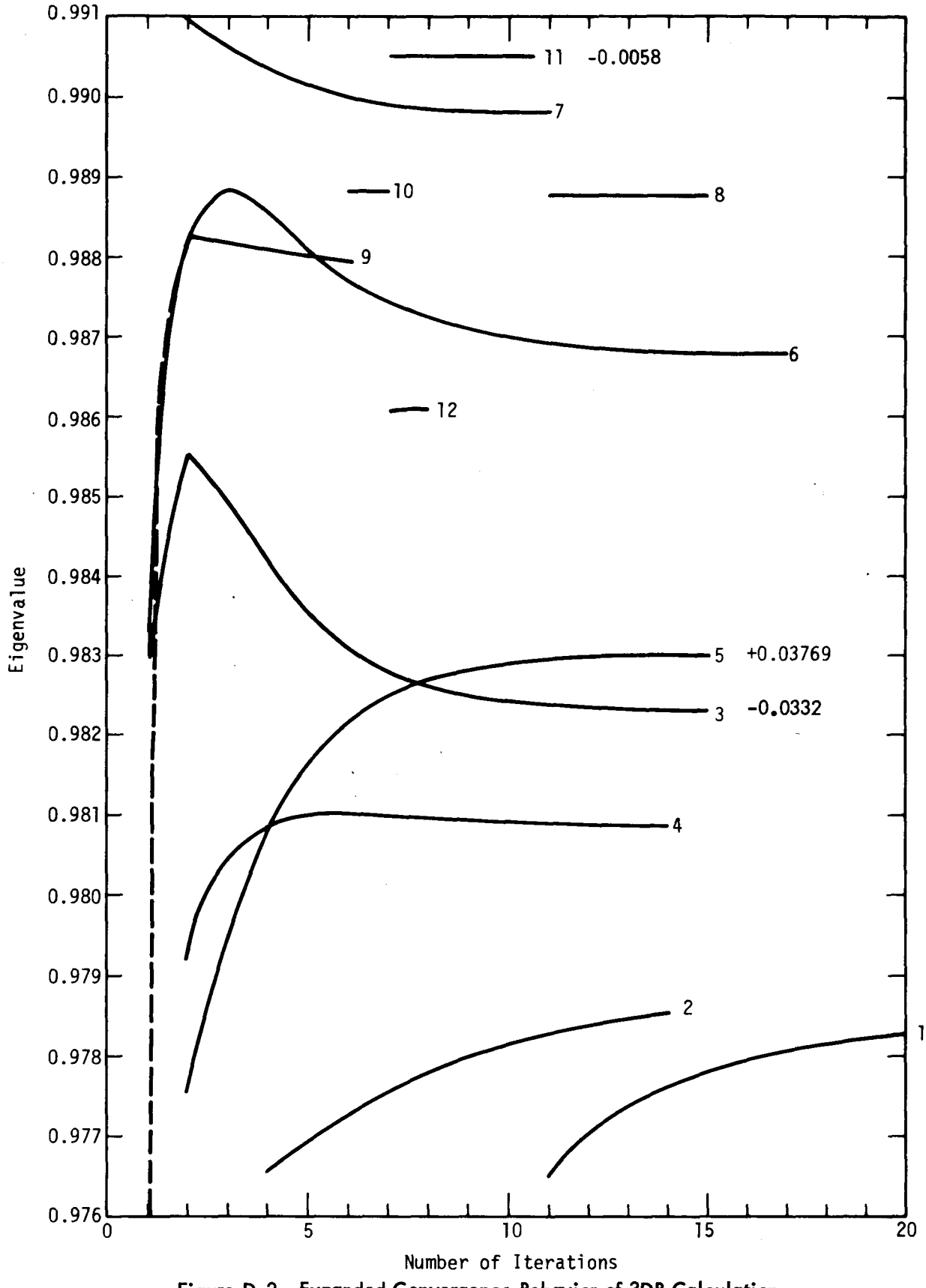

Figure D-2 Expanded Convergence Behavior of 3DB Calculations

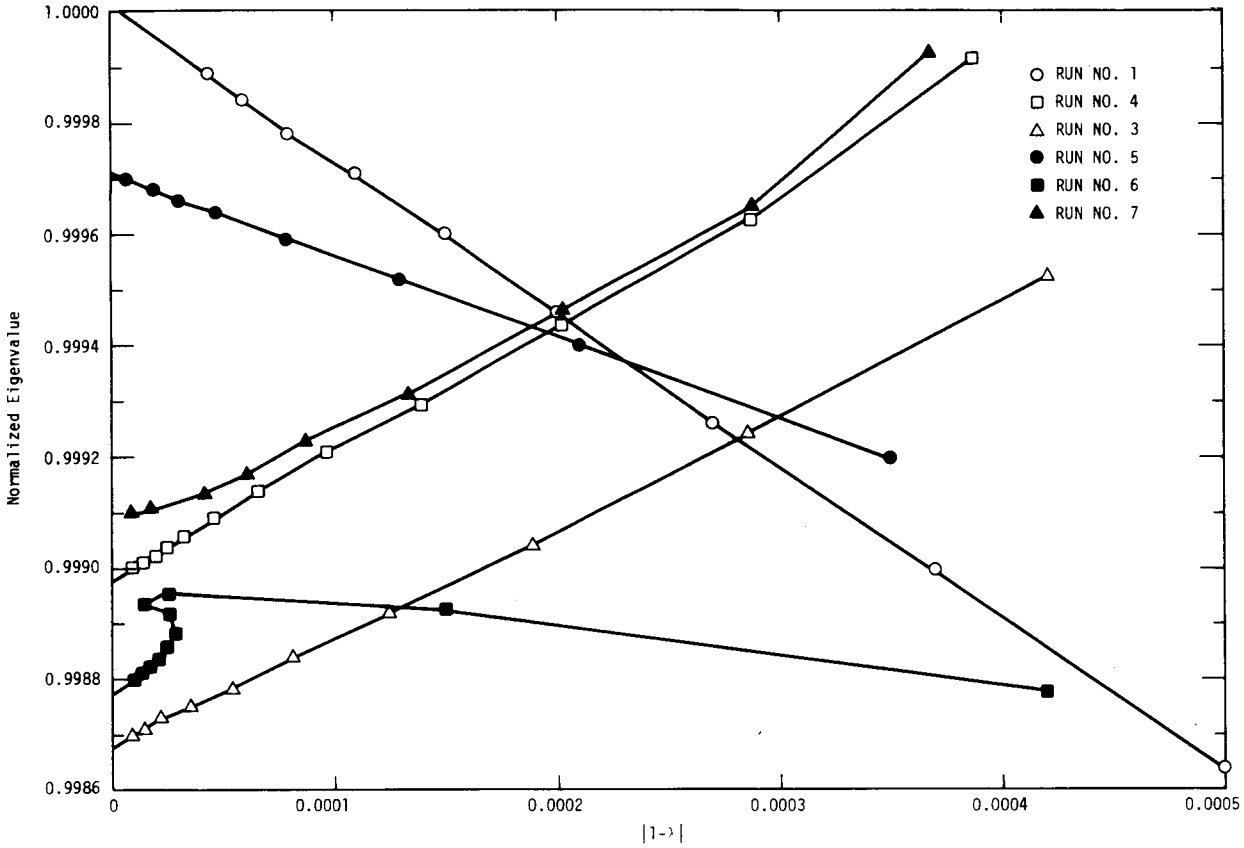

Figure D-3 Convergence plotted against $|1-\lambda|$ for four group 3DB Calculations

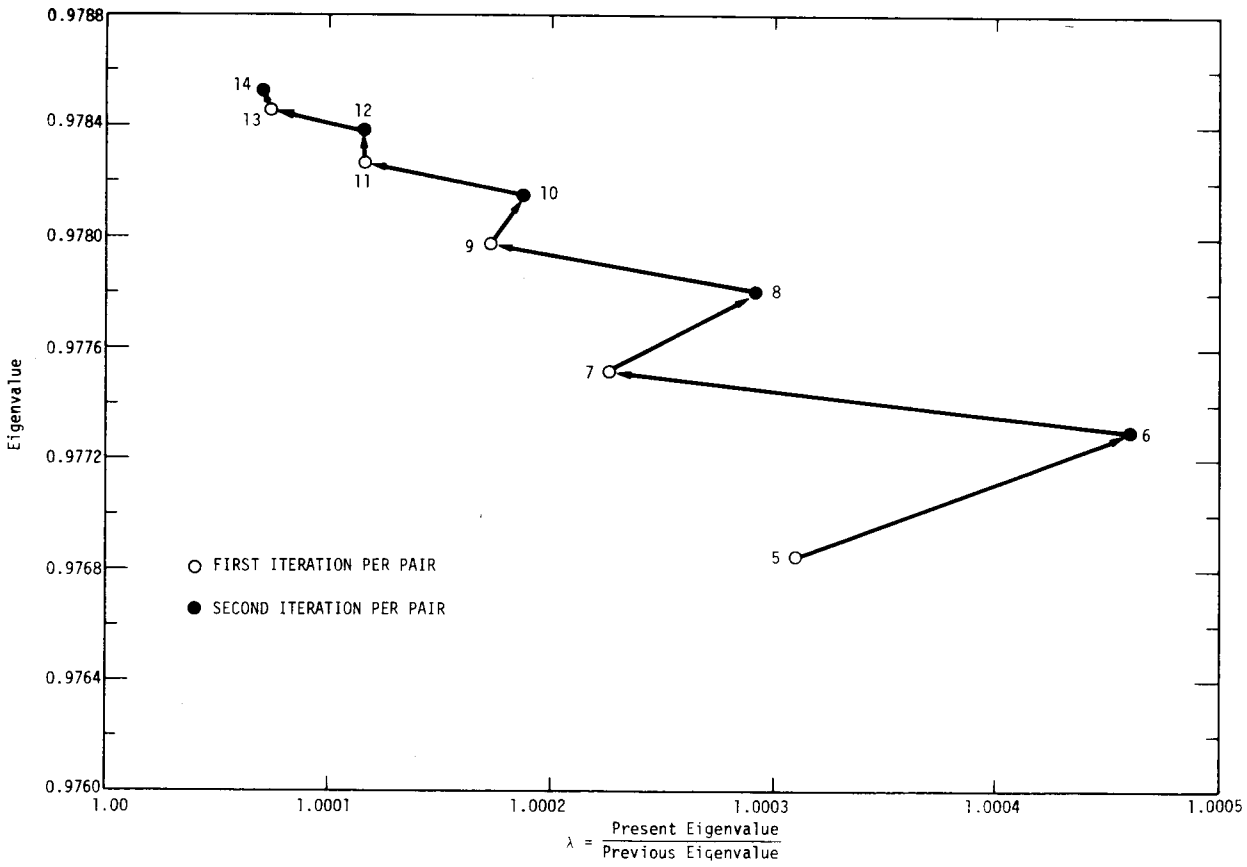

Figure D-4 Convergence plotted against $|1-\lambda|$ for thirty group 3DB Calculation in Restart Mode

DISTRIBUTION

No. of Copies

OFFSITE

21 AEC Division of Reactor Development and Technology

Director, RDT
Assistant Director, Project Management
Assistant Director, Nuclear Safety
Assistant Director, Plant Engineering
Assistant Director, Reactor Engineering
Assistant Director, Reactor Technology
FFTF Project Manager
LMFBR Program Manager
EBR-II Program Manager
Chief, Liquid Metal Projects Br
Chief, Analysis and Evaluation Br
Chief, Fast Reactor Safety Br
Chief, Fuel Recycle Br
Chief, Reactor Physics Br
Chief, Instrumentation & Control Br
Chief, Liquid Metal Systems Br
Chief, Core Design Br
Chief, Fuel Engineering Br
Reactor Physics Br
PB Hemmig
RJ Neuhold
Core Design Br
TE Murley

2 AEC Division of Technical Information Extension

5 AEC Site Representatives

Argonne National Laboratory-ID
Argonne National Laboratory-AR
Atomics International
General Electric Company
Westinghouse Electric Company

1 Aerojet Nuclear Company

P.O. Box 1845
Idaho Falls, Idaho 83401

RM Brugger

No. of Copies

2 Argonne National Laboratory

R Avery
LMFBR Program Office

1 Atomic Power Development Associates, Inc.

1911 First Street
Detroit, Michigan 48226

JB Nims

2 Atomics International

H Alter
HA Morewitz

1 Babcock & Wilcox Company

Old Forest Road
Lynchburg, Virginia 24505

DH Roy

2 Brookhaven National Laboratory

M Drake
S Pearlstein

1 Combustion Engineering, Inc.

P.O. Box 500
Windsor, Connecticut 06095
JJ Prabulos, Jr.

2 General Electric Company

Breeder Reactor Division Operation
P Greebler
B Wolfe

1 Gulf General Atomic Inc.

P.O. Box 608
San Diego, California 92112
R Dahlberg

1 Lawrence Livermore Laboratory

P.O. Box 808
Livermore, California 94550
RJ Howerton

No. of Copies

1 Los Alamos Scientific Laboratory
GH Best

2 Oak Ridge National Laboratory
AM Perry
NJ Ackerman

1 United Nuclear Corporation
Grasslands Road
Elmsford, New York 10523
JR Tomonto

3 Westinghouse Electric Corporation
Advanced Reactors Division
MW Dyos
PF Fox
RJ Slember

ONSITE HANFORD

1 RDT Site Office
FR Standerfer

2 Battelle Northwest Laboratory
LC Schmid
Technical Information Files

3 AEC, Richland Operations Office
JM Shivley
TA Nemzek
RM Poteat

ONSITE DISTRIBUTION (Cont'd)

No. of Copies	Westinghouse Hanford	
73	QL Baird	DR Marr
	RA Bennett	WJ McShane
	ET Boulette	JV Nelson (10)
	WL Bunch	BH Noordhoff
	EA Evans	LD O'Dell
	SR Fields	RP Omberg
	RM Fleischman (10)	RE Peterson
	JF Fletcher	RB Rothrock
	JG Gallagher	RE Schenter
	RW Hardie	DP Schively
	RA Harris	FA Schmittroth
	RE Heineman	AA Simmons
	RJ Hennig	A Squire
	PL Hofmann	DD Stepnewski
	JN Judy	JW Upton
	RB Kidman	AE Waltar
	HT Knight	SA Weber
	DC Kolesar	JE Werle
	FJ Leitz	Document Control (15)
	WW Little	Technical Publications (2)